REPORT No. 909

LAMINAR-BOUNDARY-LAYER OSCILLATIONS AND TRANSITION ON A FLAT PLATE[1]

By G. B. Schubauer and H. K. Skramstad

SUMMARY

This is an account of an investigation in which oscillations were discovered in the laminar boundary layer along a flat plate. These oscillations were found during the course of an experiment in which transition from laminar to turbulent flow was being studied on the plate as the turbulence in the wind stream was being reduced to unusually low values by means of damping screens. The first part of the paper deals with experimental methods and apparatus, measurements of turbulence and sound, and studies of transition. A description is then given of the manner in which oscillations were discovered and how they were found to be related to transition, and then how controlled oscillations were produced and studied in detail. The oscillations are shown to be the velocity variations accompanying a wave motion in the boundary layer, this wave motion having all the characteristics predicted by a stability theory based on the exponential growth of small disturbances. A review of this theory is given. The work is thus experimental confirmation of a mathematical theory of stability which had been in the process of development for a period of approximately 40 years, mainly by German investigators.

I. INTRODUCTION

From previous investigations, both theoretical and experimental, much is known about the laminar boundary layer. Its mean velocity distribution, thickness, and separation point may be regarded as so well understood that little further study is required. When fluctuations occur in the laminar boundary layer, their origin, character, and effect on transition from laminar to turbulent flow still present formidable problems. It has been observed, for example, that the flow in a laminar boundary layer is not steady when turbulence is present in the surrounding stream; but, beyond the simple observation that velocity fluctuations exist, little is known experimentally concerning the behavior of the fluctuations. Transition is known to depend on stream turbulence and fluctuations in the layer are believed to be the primary cause of transition, but just how the three are interrelated has never been completely understood.

Experimental evidence indicates, in some cases at least, that transition results from separation of the boundary layer caused by adverse pressure gradients; and the view has been taken by Taylor (reference 1) and other investigators that the local pressure gradients accompanying velocity fluctuations bring about transition in this way. Isotropic turbulence in the surrounding flow involves velocity fluctuations for which the pressure gradients are known when the intensity and the scale of the turbulence are specified, and relations involving this pressure gradient and transition Reynolds number that are in fair agreement with experiment have been proposed. These relations are restricted to a particular type of disturbance but are useful for expressing experimental results on the effect of isotropic turbulence.

On the purely theoretical side, attempts have been made to account for transition by stability considerations in which the growth or decay of a small disturbance is determined by the kinematic viscosity of the fluid, the thickness of the boundary layer, the speed outside the layer, and the frequency or the wave length of the disturbance. Important contributions to stability theory have been made by Tollmien (references 2 and 3) and Schlichting (references 4 to 7). Experimental evidence has so far yielded only scant support of the stability theory; and this support has come from experiments in which the flow was known to be of an unstable type, namely, the flow in a divergent channel (reference 8), in a wake at low speeds (reference 9), and in an acoustically sensitive jet (reference 10). No support has come from past wind-tunnel experiments, in which the connection between the disturbance and transition appears to be mainly through the magnitude of the disturbance. In short, the accumulated wind-tunnel results have led to the general opinion among experimentalists that the pressure gradients accompanying any disturbance in the surrounding flow cause transition when such gradients become sufficiently large. In contrast, stability theory requires that the boundary layer be either stable or unstable, depending merely on the frequency or the wave length of the disturbances present; hence, the nature of the disturbance rather than its magnitude is the essential quality. Experiment and theory have therefore led to divergent points of view and neither has fully explained the nature of transition.

In the present experiment it is hoped that the two points of view have been brought into closer accord for one of the simplest, but practical, boundary-layer problems—that of the Blasius distribution near the surface of a flat plate. The experiment was originally intended to be a general study of transition on a flat plate at zero pressure gradient under conditions of low stream turbulence, one purpose being to trace the course of transition as near as possible to vanishing turbulence. This purpose was carried out, but the appearance at low turbulence of an oscillation in the laminar boundary layer opened a new field of investigation and led to an extensive study of the phenomena termed "laminar-boundary-layer oscillations." Investigations revealed that

[1] This paper was originally issued in April 1943 as an NACA Advance Confidential Report.

the oscillations were the result of amplification of small disturbances in accordance with stability theory. When the oscillations were artificially produced, their characteristics could be studied in detail and compared with the characteristics prescribed by theory.

It seems evident from the results of this investigation that transition involves two things: One is the disturbance itself, its origin, and its behavior in the boundary layer; the other is the effect of the disturbance, either produced in the boundary layer or entering from without, in bringing about turbulent flow. Sufficiently small disturbances cannot produce transition, but a small disturbance may grow according to stability theory until it is sufficiently large to cause the flow to become turbulent. The growing process is the link between the stability theory and transition.

In most of the earlier investigations, observations of the transition point were made but little or no effort was made to observe disturbances in the boundary layer before transition. The first known observations of velocity fluctuations in the laminar boundary layer were made by Dryden (reference 11) but, in his experiment as in most others, the initial disturbances were so large that transition occurred after only a small growth. Nikuradse (reference 12) attempted to test the stability theory by producing sinusoidal fluctuations in the boundary layer near the leading edge of a flat plate in water; but the results were inconclusive, partly because the artificial fluctuations, as well as general disturbances, were too large and partly because observations were limited to the determination of transition points.

The results obtained in the present investigation can be attributed largely to the low level of turbulence in the wind stream and to the careful study made of velocity fluctuations throughout the laminar boundary layer. Hot-wire anemometers of high sensitivity and of special design made such an investigation possible.

The work was conducted at the National Bureau of Standards under the sponsorship and with the financial assistance of the National Advisory Committee for Aeronautics. The investigation of transition on a flat plate at low turbulence was suggested by Dr. Hugh L. Dryden, and the authors wish to acknowledge his assistance and many valuable suggestions in connection with the experimental program.

II. SYMBOLS

x	distance from leading edge of flat plate
y	distance from surface of flat plate
U_0	mean velocity outside boundary layer
U	mean velocity at a point in boundary layer
u	instantaneous x-component of fluctuation velocity
v	instantaneous y-component of fluctuation velocity
w	instantaneous fluctuation velocity perpendicular to U_0 and parallel to surface of flat plate
u', v', w'	root-mean-square values of u, v, and w, respectively
c_r	wave velocity
$\beta_r=2\pi f$	
f	oscillation frequency
$\alpha=2\pi/\lambda$	
λ	wave length
β_i	amplification coefficient
ρ	density
μ	viscosity
ν	kinematic viscosity (μ/ρ)
q	dynamic pressure
δ	boundary-layer thickness
δ^*	boundary-layer displacement thickness
	$\delta^*=1.72\sqrt{\frac{\nu x}{U_0}}$ for Blasius velocity distribution
	$\delta^*=0.341\delta$ relation used by Tollmien and Schlichting (references 2, 4, and 5)
R	Reynolds number ($U_0\delta^*/\nu$)
R_x	x-Reynolds number (U_0x/ν)
	$R=1.72\sqrt{R_x}$ for Blasius velocity distribution
Λ	Kármán-Pohlhausen parameter $\left(\frac{dU_0}{dx}\frac{\delta^*}{\nu}\right)$

III. APPARATUS AND METHODS

1. WIND TUNNEL

The present investigation was conducted in the 4½-foot wind tunnel at the National Bureau of Standards. The general layout of the tunnel is shown in figure 1. The flat plate was located vertically in the test section with the leading edge 6 feet from the upstream end. In order to reduce vibration, the test section of this tunnel is supported directly from the foundation and is joined to the rest of the circuit by only

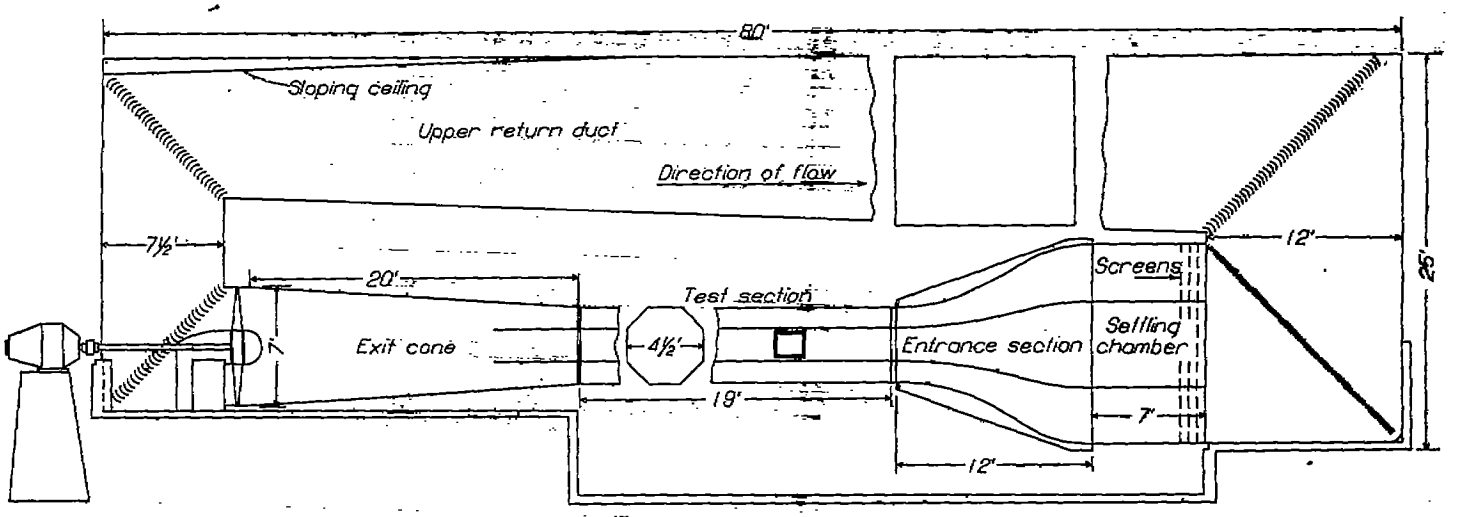

FIGURE 1.—Elevation view of 4½-foot wind tunnel.

a sponge-rubber seal at each end. The area reduction from settling chamber to test section is 7.1:1. The guide vanes ahead of the settling chamber were made finer than the others in order to reduce the scale of the turbulence and to permit as much reduction in turbulence through decay as possible. Since directional fluctuations in the horizontal plane were found to be large, closely spaced straighteners were placed at right angles to and on top of the fine guide vanes. This combination was in effect a honeycomb and resulted in great improvement in the steadiness of the stream. Further reduction of turbulence was obtained by installing damping screens in the settling chamber. Without screens, the turbulence in the test section was 0.27 percent at 100 feet per second and, with seven screens, was 0.032 percent.

2. FLAT PLATE

The flat plate was a commercial sheet of aluminum ¼ inch thick, 4½ feet wide, and 12 feet long. The leading edge, which was symmetrical and pointed, was formed by the intersection of circular arcs tangent to the original surface 4 inches from the leading edge. The surface was left in its original condition and had a mirrorlike finish, marred slightly by small scratches barely perceptible to the fingertips. Waviness was quite perceptible when viewed near grazing incidence. A surface gage showed variations from approximately 0.01 to 0.02 inch over distances from 1 to 2 feet. These were bends in the plate evidently produced by the rolling process.

The plate was bolted along the top and the bottom edges to one side of 3-inch steel channels, which were in turn bolted to the floor and to the ceiling of the tunnel. The flanges away from the plate served as rails at the floor and at the ceiling for a carriage on which all exploring apparatus was mounted. The carriage was simply a steel plate ⅜ inch thick and 6 inches wide, with runners and guides at the ends in contact with the rails. This plate was thus parallel to the wind and 3 inches from the flat plate. All explorations in the boundary layer were made 25 inches or more ahead of the carriage to avoid the local pressure field. The carriage was propelled by hand from the outside of the tunnel by a sprocket and chain.

3. CONTROL OF PRESSURE DISTRIBUTION

In order to control the pressure gradient along the flat plate, the cross section of the working chamber was varied by adjustable auxiliary walls on the vertical sides of the chamber. These walls were aluminum sheets ⅛ inch thick and 22 inches wide extending from opposite the trailing edge of the plate to a distance 4 feet ahead of the leading edge. The sheets, mounted on screws spaced 9 inches and threaded through the tunnel walls, were adjustable to and from the sides of the tunnel. In order to prevent discontinuity at the top and at the bottom edges, the sheets were backed by a stretched rubber diaphragm; the combination of aluminum sheet and rubber formed a continuous flexible wall that could be warped or displaced as desired. The maximum range of displacement of these auxiliary walls was about 4 inches.

By this means the pressure could be made to rise, to fall, or to remain constant along the plate. (See curves A, B, and C, fig. 30.) For most of the experiment the walls were set for zero pressure gradient.

The provision for warping the walls into a bulge or a hollow did not prove so useful as was anticipated because the effect of the warp usually extended over too great a distance to give the desired result. When it was desired to produce a sharp pressure rise or fall, other devices were used. For example, an airfoil extending from floor to ceiling near the plate produced a sharp pressure fall followed by an abrupt rise. A pressure fall without a rise was easily produced by proper blocking of the stream.

Although measurements were taken on only one side of the flat plate, the auxiliary walls on each side of the tunnel were given the same shape for symmetry. Some asymmetry nevertheless existed because of the presence of the carriage and the measuring equipment on only one side of the plate. Although this resulted in greater blocking of the stream on the working side, it was found that some excess blocking here was necessary to direct the flow at a slight angle to the leading edge of the plate so that the stagnation point was displaced slightly from the sharp edge to the working side of the plate. The transition point was unaffected by the position of the stagnation point so long as this point was not displaced to the opposite side of the plate. The slight excess blocking was therefore maintained at all times to prevent directional variations accompanying the turbulence in the stream from ever carrying the stagnation point to the opposite side.

4. MEASUREMENT OF PRESSURE DISTRIBUTION AND DETERMINATION OF TRANSITION POINT

A small pitot-static head was arranged as shown in figure 2 with the impact tube in contact with the surface and the static tube parallel to the stream ¼ inch from the surface. This combination was carried on an arm attached to the carriage 28 inches to the rear and could slide fore and aft with forklike guides and impact tube always in contact with the surface. Both tubes were made from thin-wall nickel tubing

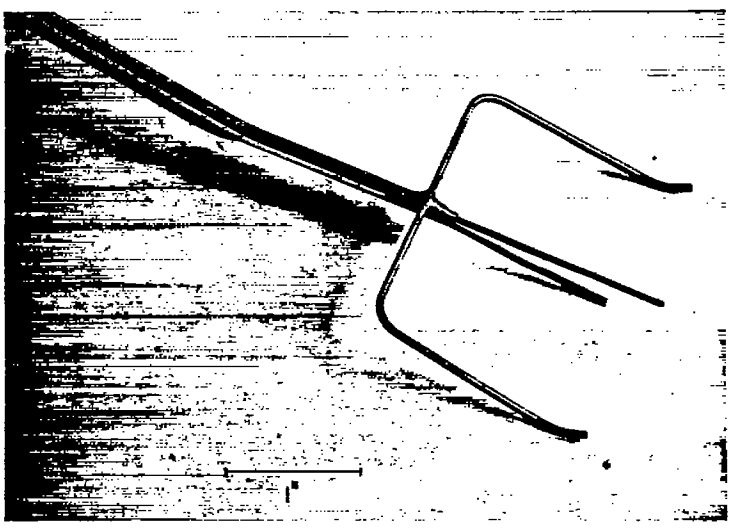

FIGURE 2.—Pitot-static surface tube used to measure pressure distribution and position of transition.

with 0.04-inch outside diameter. The impact tube was flattened on the end to form a slit 0.007 inch wide, the center of which was 0.006 inch from the surface when the tube was in contact. The static tube had four 0.008-inch holes drilled through the wall, 8 diameters from the closed end.

Only the static tube of this instrument was used when pressure distributions were measured and both tubes were used when transition points were determined. Traverses were always horizontal and usually made along the center line of the plate. The static pressure was thus measured ¼ inch from the surface, which for most of the surface corresponded to a position outside the boundary layer. A large variation of pressure normal to the surface was found near the leading edge where the pressure distribution was determined by the shape of the leading edge. Also, pressure effects caused by waviness of the surface depended on the distance from the surface. Since the former variations were confined to the first 6 inches from the leading edge and the latter were small, variations in pressure in the ¼-inch distance normal to the surface were neglected.

The detection of transition by the surface-tube method depends on the variation with x of impact pressure near the surface, which corresponds closely to the variation of shearing stress at the surface. This impact pressure decreases with distance from the leading edge to the beginning of transition, then rises through the transition region, and again falls in the turbulent region. In the present work, the point of minimum pressure was taken as the beginning of transition and the point of maximum pressure following the rise was taken as the point where turbulence was fully developed.

5. DETERMINATION OF BOUNDARY-LAYER THICKNESS

Velocity distributions across the boundary layer were determined by traversing normal to the surface with a flattened impact tube similar to the surface tube. This tube was carried on an arm similar to the one shown with the hot-wire anemometer attached in figure 3. Both the micrometer

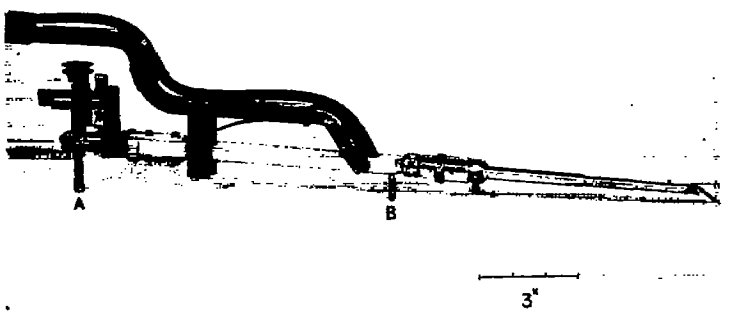

FIGURE 3.—Apparatus for traversing normal to the surface. Hot-wire head attached.

screw A and the fulcrum B were held in contact with the surface of the plate by the rigid arm extending rearward to the carriage, and motion of the impact tube to and from the surface was obtained by rocking the arm about the fulcrum by means of the screw. The velocity distributions were used to determine δ^*. When the pressure gradient was zero, the measured values of δ^* were in agreement with those calculated by the Blasius formula

$$\delta^*=1.72\sqrt{\frac{\nu x}{U_0}}$$

Whenever the value of δ^* was needed for presenting results obtained at zero pressure gradient, the value calculated by this formula was used.

Tollmien and Schlichting (references 2, 4, and 5) used a constant in the above formula equal to 1.73 for computing δ^*. More recent values of the constant are 1.7207 given by Dryden (reference 11) and 1.7208 given by Goldstein (reference 13). A value of 1.72 is therefore used in the present work.

6. HOT-WIRE TURBULENCE EQUIPMENT

A variety of apparatus, such as amplifiers, bridges, potentiometers, oscillators, oscillographs, and numerous types of hot-wire anemometer, comes under the heading of hot-wire equipment for measuring turbulence. Amplifiers with attendant power supplies and hot-wire anemometers are usually special equipment, whereas the other equipment is of standard commercial design. Amplifiers used in turbulence work and circuits to compensate for the thermal lag of hot wires have, however, been standardized to a certain extent and their essential features are described in the literature. Two amplifiers, which were designed and built by W. C. Mock, Jr., were used in the present investigation. One of the amplifiers is described in reference 14; the other was a newer and more portable type with about the same frequency response but using capacitance compensation instead of inductance compensation. Both types of compensation and the requirements to be met by each type are described in reference 15. The theory of compensation is given in reference 16. When properly compensated, the over-all response of wire and amplifiers was uniform from 3 to about 2000 cycles per second.

In all cases hot-wire anemometers must be calibrated by measuring the voltage across the wire at known airspeeds; or, if the anemometer is sensitive to direction changes, it must be calibrated by measuring the voltage at several angles to the wind. For this purpose a potentiometer is necessary. A Wheatstone bridge must be used to obtain the resistance of the wire at air temperature. Throughout the present work, both in calibration and in use, the heating current was held constant and only the temperature and the voltage across the wire were allowed to vary. This condition was maintained during rapid velocity fluctuations by a sufficiently large choke coil in series with the wire. Amplifiers were calibrated by applying to them a known alternating voltage from an oscillator. By use of the calibration data, velocity fluctuations could be calculated from the amplified and properly compensated voltage fluctuations across the hot wire. A cathode-ray oscillograph was used for visual observation of fluctuations and also for making photographic records with a moving-film camera. When observations were simultaneously taken on two wires, an electronic switch was used in conjunction with the oscillograph.

7. HOT-WIRE ANEMOMETERS

The hot-wire anemometers used here may be divided into two classes: (1) Those used in the free stream to measure turbulence; (2) those used in the boundary layer to study oscillations, transition phenomena, and turbulence. Anemometers of class (1) were designed for high sensitivity and for freedom from vibrational effects. Anemometers of class (2) were designed for working near a surface with a minimum of interference and with as little vibrational motion relative to the surface as possible. Both types used platinum wire 0.00025 inch in diameter, obtained by etching the silver coating from Wollaston wire. The etched wire was soft-soldered to prongs made either from fine sewing needles or from fine copper wire. Platinum wires of this size were adequately sensitive in lengths no greater than $\frac{1}{16}$ inch and, in the range of operating conditions, had time constants ranging from 0.0005 to 0.002 second.

Anemometers of class (1) were made with a single wire normal to the wind for measuring u' or with two wires set at an angle to the wind in the form of an X for measuring v' and w'. Heads of these two types are shown in figure 4.

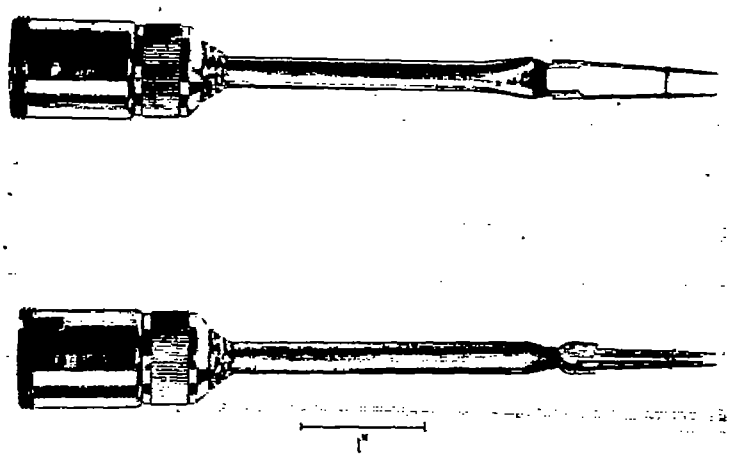

FIGURE 4.—Hot-wire heads for the measurement of free stream turbulence.

Both have platinum wires (not visible in the photograph) across the tips of the prongs; the four-prong head has the two wires forming an X. In the X-arrangement the wires lie as nearly as possible in a plane without touching and subtend an angle of 60° with each wire at an angle of about 30° to the wind. Braces of silk thread cemented across the prongs about $\frac{1}{4}$ inch from the tips were necessary to prevent wire breakage. All wires were about $\frac{1}{16}$ inch long. These arrangements of wires take advantage of the directional characteristics of a wire in order to obtain sensitivity to the component desired. The sensitivity of a wire to direction is known to depend on the angle to the wind, being zero when normal and again when parallel. Sensitivity to u is a maximum when the wire is normal. Since v and w are small, their principal effect is to cause fluctuation in direction of the stream when added vectorially to U and the effect on the magnitude of the instantaneous velocity is insignificant. A wire normal to the wind responds thus to u-fluctuations rather than to v or w.

An X-arrangement of two identical wires, each making the same angle to the wind, with voltage opposed produces a resultant voltage change only when the wires are differentially cooled. This arrangement is then insensitive to u but highly sensitive to direction changes in the plane of the wires and hence to v or to w depending on the orientation of the plane. When fluctuations are large, isolation of single components in this way is not complete and voltage changes are not exactly proportional to velocity changes. If the fluctuations do not exceed 5 percent of the mean speed, errors from these sources are believed to be less than 1 percent.

The mountings for the hot-wire heads are shown in figure 5. The central member to which the head is attached is held

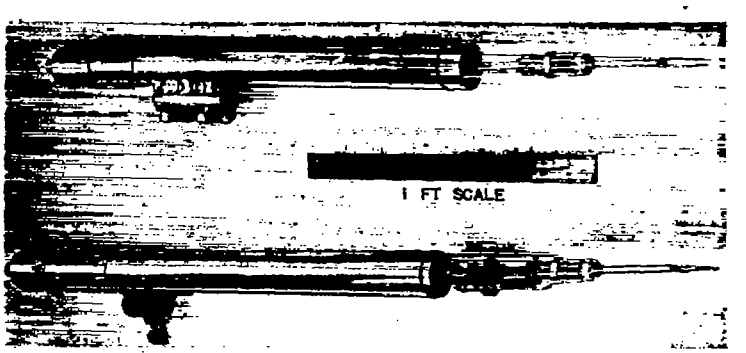

FIGURE 5.—Rubber-suspension type mountings with hot-wire heads attached.

within the cylindrical tube by a rubber-band suspension and in this way is isolated from vibration from the tunnel walls. Vibrational effects were not troublesome after a sufficiently "soft" suspension of this sort was used. The mounting for the X-wires contains an angle-changing device for calibrating the wires.

In the boundary layer only the u-component was measured, except when one attempt was made to discover whether the boundary-layer oscillations had a w-component. A study of v was considered desirable but no appropriate hot-wire head of sufficiently small dimensions was available for the purpose. For anemometers of class (2), therefore, most attention was given to hot-wire heads with the wire normal to the wind and parallel to the surface. The wire length was usually 0.04 inch. For traversing along the surface with the wire at a fixed distance, the wire was attached at the tips of prongs extending about $\frac{1}{4}$ inch forward from a small celluloid sled, which was held against the surface by wire springs from a brass tube attached to the carriage. A sled assembly with two pairs of prongs for supporting two wires at different distances from the surface is shown in figure 6. Another sled was also used with two hot wires making a V in a plane parallel to the surface. The latter arrangement was sensitive to w. The sled was believed to be the best possible type of hot-wire head to prevent relative motion between the wire and the surface. Interference effects were found negligible.

For traversing normal to the surface, the hot wire was supported on the tips of steel sewing needles extending into the boundary layer from the arm of the traversing apparatus shown in figure 3. This arrangement was made sufficiently rigid to be free from vibration troubles but was not appropriate for traversing parallel to the surface. A combination of this apparatus with a sled was used when it was desired

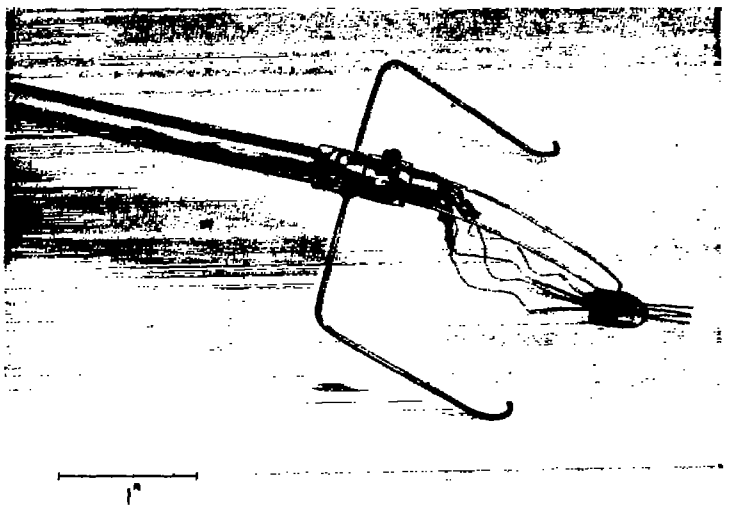

FIGURE 6.—Sledlike hot-wire head arranged for two hot wires.

to keep one wire at a fixed distance from the surface while moving the other in and out from the surface.

IV. REDUCTION OF STREAM TURBULENCE AND EFFECT ON REYNOLDS NUMBER OF TRANSITION AT ZERO PRESSURE GRADIENT

In the present investigation, effects of high stream turbulence were of little concern. Emphasis was placed rather on reducing the turbulence as far as practicable in order to study the boundary layer when it was as little disturbed from the stream as possible. The turbulence was successively reduced by placing various numbers and combinations of damping screens in the settling chamber. For each addition of a screen and for every recombination of screens, measurements were made of u'/U_0, v'/U_0, and w'/U_0 in the working chamber and the values of R_x at the beginning and at the end of transition were determined.

No correction for wire length according to the method given in reference 17 was made, since the appropriate scale for v' and w' could not be determined. If the probable order of magnitude of the scale is considered, the correction is small and is believed to be unimportant in view of the accuracy attainable in the measurement of low turbulence.

Screens of fine mesh and small wire were used in order that the turbulence produced by the screen itself would decay rapidly. Each screen completely covered the cross section of the settling chamber and, when more than one screen was used, a spacing of 6 inches or more was allowed between them. Preliminary surveys with the hot-wire anemometer showed that the turbulence was uniform over the usable cross section of the stream and that little or no decrease in turbulence occurred in the length of the working chamber. The turbulence could therefore be specified by hot-wire measurements made at one point in the working chamber. The measurements showed that v' and w' were nearly equal to each other but generally greater than u'. This nonisotropic condition is known to be caused by the contraction of the stream from the large area of the settling chamber to the smaller area of the working chamber. The more the turbulence was reduced by the addition of screens, the less this difference became and, finally, near the lowest turbulence u' was actually larger than v' and w'. In all cases the turbulence increased with the wind speed, an effect that could be partly accounted for by the decreasing resistance coefficient of the screens with increasing speed.

TABLE I

TURBULENCE WITH SIX DAMPING SCREENS IN SETTLING CHAMBER

[Measurements at single station in working chamber]

U_0 (fps)	$\frac{u'}{U_0}$ (percent)	$\frac{v'}{U_0}$ (percent)	$\frac{w'}{U_0}$ (percent)	$\frac{\sqrt{\frac{1}{3}(u'^2+v'^2+w'^2)}}{U_0}$ (percent)
30	0.019	0.011	0.012	0.0145
40	.021	.020	.019	.0200
50	.024	.023	.020	.0224
60	.027	.026	.021	.0248
70	.030	.030	.026	.0287
80	.033	.035	.032	.0334
90	.035	.039	.037	.0371
100	.037	.042	.041	.0401
110	.040	.044	.045	.0430
120	.045	.046	.047	.0459

As the number of screens was increased, a reduction in turbulence was obtained with each additional screen but by successively decreasing amounts; and the reduction by this means appeared to have reached a practicable limit when six screens were installed. The measured values with six screens are given in table I. It was believed at first that a level had been reached nearly equal to the turbulence produced by the screens themselves. A finer screen than any of the others was therefore added downstream from the six screens already present. Since no screens with finer wires than those already used were commercially available, a screen made from silk bolting cloth was installed. Some further reduction was obtained but not so much as was expected. No attempt was made at further reduction. The

TABLE II

TURBULENCE WITH SIX DAMPING SCREENS FOLLOWED BY ONE BOLTING CLOTH IN SETTLING CHAMBER

[Measurements at single station in working chamber]

U_0 (fps)	$\frac{u'}{U_0}$ (percent)	$\frac{v'}{U_0}$ (percent)	$\frac{w'}{U_0}$ (percent)	$\frac{\sqrt{\frac{1}{3}(u'^2+v'^2+w'^2)}}{U_0}$ (percent)
30	0.018	0.012	0.009	0.0135
40	.019	.012	.010	.0142
50	.021	.014	.015	.0169
60	.026	.018	.016	.0204
70	.029	.020	.017	.0226
80	.033	.022	.018	.0251
90	.037	.026	.020	.0286
100	.040	.029	.023	.0315
110	.044	.034	.026	.0353

measured values of the turbulence at this lowest level are given in table II. The x-Reynolds numbers of transition found during the various stages of reduction are shown in figure 7. The highest turbulence shown in the figure (0.342 percent) was obtained by placing a square-mesh grid of ½-inch rope, spaced 6 inches, in the settling chamber a few inches downstream from the set of six wire screens. The transition point found by Hall and Hislop (reference 18) for their lowest turbulence is indicated in figure 7. By

definition, their transition point corresponds to the beginning of transition in the present paper.

Two questions are raised by the foregoing results: (1) Why was the addition of the bolting-cloth screen so ineffective in further reducing the turbulence, and (2) why was transition on the flat plate unaffected by reduction of tur-

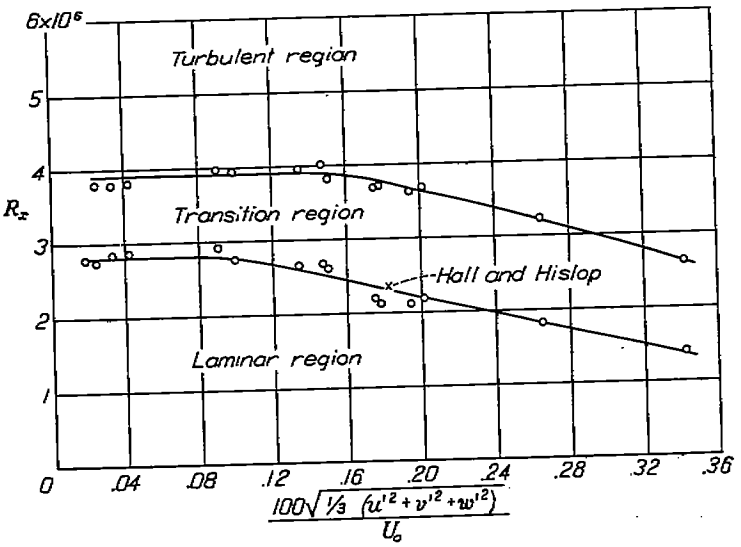

FIGURE 7.—Effect of turbulence on x-Reynolds number of transition. Flat plate; zero pressure gradient.

bulence below about 0.08 percent? The first question is answered in the following section. The second question is more difficult and an attempt will be made to answer it only after boundary-layer oscillations are considered. (See section IX.)

V. RESIDUAL TURBULENCE AND NOISE

While the measurements of the lowest turbulence were in progress, it was noted by the trace on the screen of a cathode-ray oscillograph that the velocity fluctuations did not have the random character usually ascribed to turbulence. Vibration of the hot-wire mounting was suspected but was ruled out since changes in the softness of the mounting failed to change the appearance of the trace. Consideration was next given to the effect of wind-tunnel noise and led to the startling conclusion that a reasonably loud sound could involve particle velocities sufficient to produce an apparent turbulence of the order of that actually found. For example, a calculation based on a plane wave with an intensity of 105 decibels above a base level of 10^{-9} erg per square centimeter per second showed a root-mean-square particle velocity of 0.028 foot per second. At a wind velocity of 100 feet per second, this is equivalent to an apparent turbulence of 0.028 percent, while the measured turbulence was 0.0315 percent. A few measurements of intensity with a sound meter connected to a crystal microphone showed that the noise level was probably between 105 and 110 decibels at 100 feet per second. Since 110 decibels is equivalent to an apparent turbulence of 0.051 percent, the noise could account for the entire hot-wire reading at this speed. At the lower speeds, however, the noise intensity appeared insufficient to account for the measured turbulence. Since the wave pattern in the tunnel was very complex, calculations based on plane waves can be at best only rough approximations. Furthermore to avoid the direct effect of the wind on the microphone, it was necessary to measure the sound level at a distance from the hot wire.

An analysis was made by a wave analyzer of the spectrum of the noise from the tunnel picked up in the tunnel control room by the crystal microphone. A similar analysis was then made of the output from the hot wire in the wind tunnel. In both cases the wind velocity was 80 feet per second. A comparison of the two spectrums is shown in figure 8. Since the distribution of intensity with frequency is compared here, uncertainties in absolute intensity are of minor importance. The similarity of the curves indicates that, at a wind velocity of 80 feet per second, a large part of the hot-wire output is derived from noise.

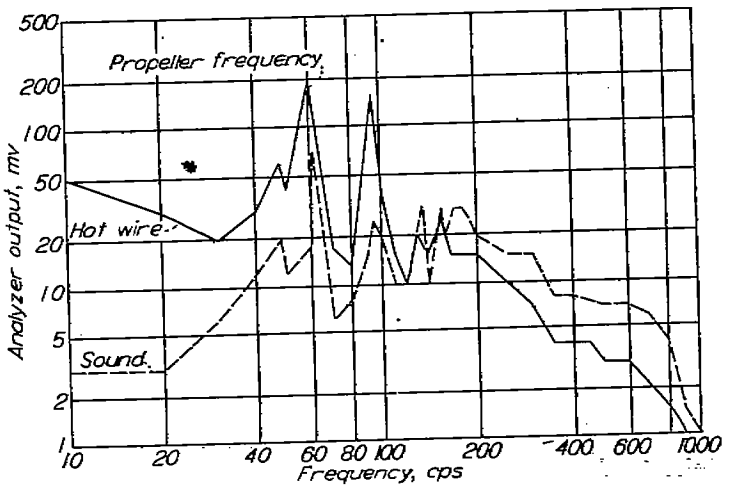

FIGURE 8.—Distribution with frequency of u-component of turbulence and sound. Wind speed, 80 feet per second; u'/U_0 (total) = 0.033 percent.

The values of turbulence in tables I and II probably contain a significant contribution from noise, especially at the higher velocities. A large part of the increase with velocity is probably due to noise. Also, a u' greater than v' and w' is evidence that not all the contributing fluctuations were carried with the stream through the entrance cone. Since most of the noise comes from the propeller, it is obvious that damping screens can reduce only the true turbulence. On the other hand, the addition of screens must increase the noise because of the higher propeller speed needed to maintain a given wind velocity through the added resistance in the screen. These facts afford a satisfactory explanation of the effective limit of damping screens in the present tunnel.

Figure 8 also suggests some information concerning the answer to the second question posed in section IV regarding the effect of turbulence on transition. Since the spectrum of this apparent turbulence is unlike that of isotropic turbulence (reference 19), such turbulence will probably affect transition in a different manner from isotropic turbulence. Velocity fluctuations from sound involve pressure changes not related to those of turbulence and involve motions correlated over great distances. Since the proportion of noise to turbulence was increased with each reduction of turbulence, anomalous transition effects are to be expected.

VI. LAMINAR-BOUNDARY-LAYER OSCILLATIONS, ZERO PRESSURE GRADIENT

1. FIRST EVIDENCE OF OSCILLATIONS

When the stream turbulence had been reduced to nearly its lowest level with the six wire damping screens, it was decided to investigate the velocity fluctuations in the laminar boundary layer itself. For this purpose one of the sledlike heads with a wire sensitive to u was arranged to slide along the surface with the wire 0.023 inch from the surface. With greatly reduced stream turbulence, it was expected that the slow irregular fluctuations, reported for a much more turbulent stream in reference 11, would be correspondingly reduced. Such fluctuations were, in fact, almost nonexistent; but, as the wire was moved downstream through the boundary layer, a regular oscillation appeared, weak at first but with increasing amplitude as the distance downstream increased. Just ahead of the transition, bursts of very large amplitude occurred and, at the initial point of transition, these bursts were accompanied by a breaking into an irregular high-frequency fluctuation characteristic of turbulence. Records of the oscillations were made by photographing the screen of the cathode-ray oscillograph with a moving-film camera. Two sets of such records are reproduced as figures 9 and 10. Figure 9 shows the progressive development of the oscillations. The traces at 6.25 and 6.5 feet already show the bursts of large-amplitude oscillations interspersed with highly disturbed turbulent motion. The final record at 8 feet indicates a completely turbulent boundary layer. The frequency of the oscillations may be judged by the $\frac{1}{10}$-second timing dots. The same phenomenon at a lower wind speed and at a greater distance from the leading edge of the plate is shown in figure 10. Here the amplifier gain (magnification) was adjusted to keep the recorded amplitude the same from position to position in order to bring out the weak as well as the strong oscillations. Attention is called to the lower oscillation frequency corresponding in this case to the lower speed and to the thicker boundary layer.

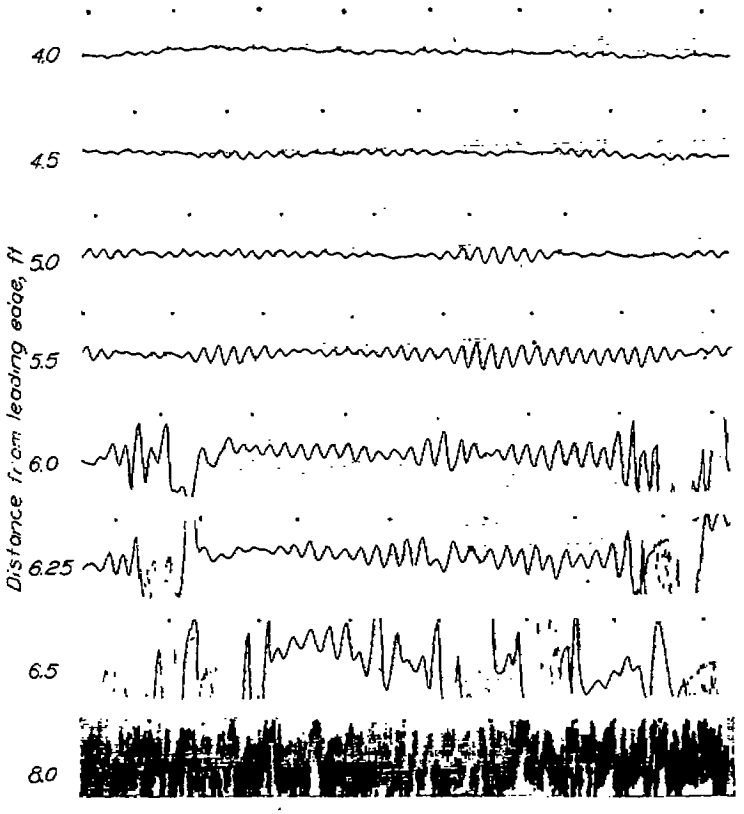

FIGURE 9.—Oscillograms of u-fluctuations showing laminar boundary-layer oscillations in boundary layer of flat plate. Distance from surface, 0.023 inch; U_0=80 feet per second; time interval between dots, $\frac{1}{10}$ second.

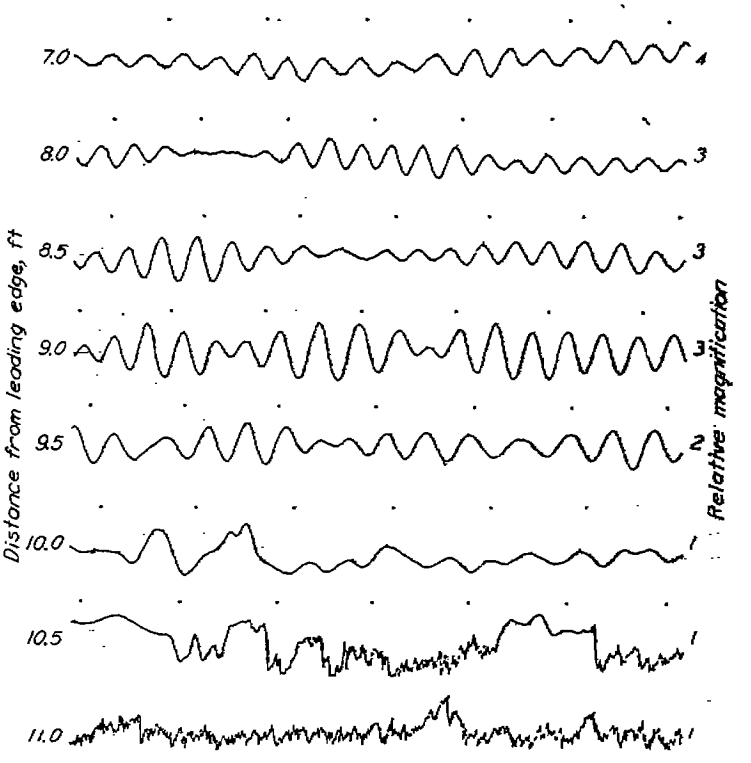

FIGURE 10.—Oscillograms of u-fluctuations showing laminar boundary-layer oscillations in boundary layer of flat plate. Distance from surface, 0.023 inch; U_0=53 feet per second; time interval between dots, $\frac{1}{10}$ second.

It was thought at first that these oscillations might possibly be due to vibration of the wire that gave rise to relative motion between the wire and the surface. This was soon ruled out since changes in the hot-wire head and support failed to cause any change in the oscillations. Furthermore, the oscillations appeared to be definitely connected with transition since the zone in which they occurred always preceded transition and moved with it fore and aft along the plate as the wind speed was varied. It could not be said with certainty that the oscillations were the cause of transition, since there existed the possibility that the boundary layer became shock-excited by transition occurring a short distance downstream, giving rise to an oscillation that was possibly the result of transition rather than the cause. The latter explanation was ruled out by removing transition with an abrupt pressure drop and yet leaving the oscillations totally unchanged at an upstream position. The alternative conclusion, with no evidence to the contrary, was that transition resulted from the growing of the oscillations to the point where the boundary layer was so highly disturbed that transition occurred.

It was soon found that the hot wire could be placed at any cross section of the boundary layer to pick up the oscilla-

tions, although the amplitude quite evidently varied with position. The frequency remained the same throughout the section except very near the surface where there was a suggestion of frequency doubling on the low-velocity part of the cycle. This effect at the 4-foot position is shown in figure 11. Since the hot wire responds to negative velocities as though they were positive, the doubling was believed to indicate that the amplitude of the oscillation was sufficiently high to reverse the direction of flow during half of each cycle.

A V-wire, sensitive to w, revealed a w-component in the oscillations. Little work was done with this wire and the relative amplitudes of u and w were not compared. With the one exception cited here, all work was done with wire sensitive to u. Because of experimental difficulties no attempt was made to detect the v-component, although it is shown by theoretical considerations in section VI, 2, that a v-component must exist. The presence of the w-component thus indicates that the oscillations were three-dimensional.

Because the effects of noise were so much in evidence, it might be supposed that the oscillations were a resonant acoustic phenomenon arising from some frequency in the sound spectrum. Among the evidence against this supposition is that presented in figure 12, which shows the effect of a tenfold increase in turbulence produced by the rope grid in the settling chamber downstream from the six damping screens. With the higher turbulence, it is seen that oscillations are present where they were absent before. It thus appears that disturbances in the stream, possibly acoustic as well as turbulent, give rise to oscillations which are not themselves sound waves.

It was believed almost from the start that the oscillations were amplified disturbances, their purity resulting from selective amplification of a single frequency or, at most, a narrow band of frequencies. Theories had been advanced to account for just such an amplification but were often ignored in experiment because no conclusive evidence in their support had been found. In order to test whether these were in reality the amplified oscillations predicted by theory, frequencies were determined from numerous oscillograms, taken at as many positions and speeds as possible and plotted in an appropriate manner on a diagram derived from the theoretical results of Schlichting. The diagram with the experimentally determined points is shown in figure 13. This figure will be made clear by the theoretical discussion in section VI, 2, and will be described in detail in section VI, 3. For the present, it is sufficient to observe that the experimental points are distributed along branch II of the theoretical curve, which is the region in which the points should fall if the initial disturbances, out of which oscillations grew, have received approximately their maximum am-

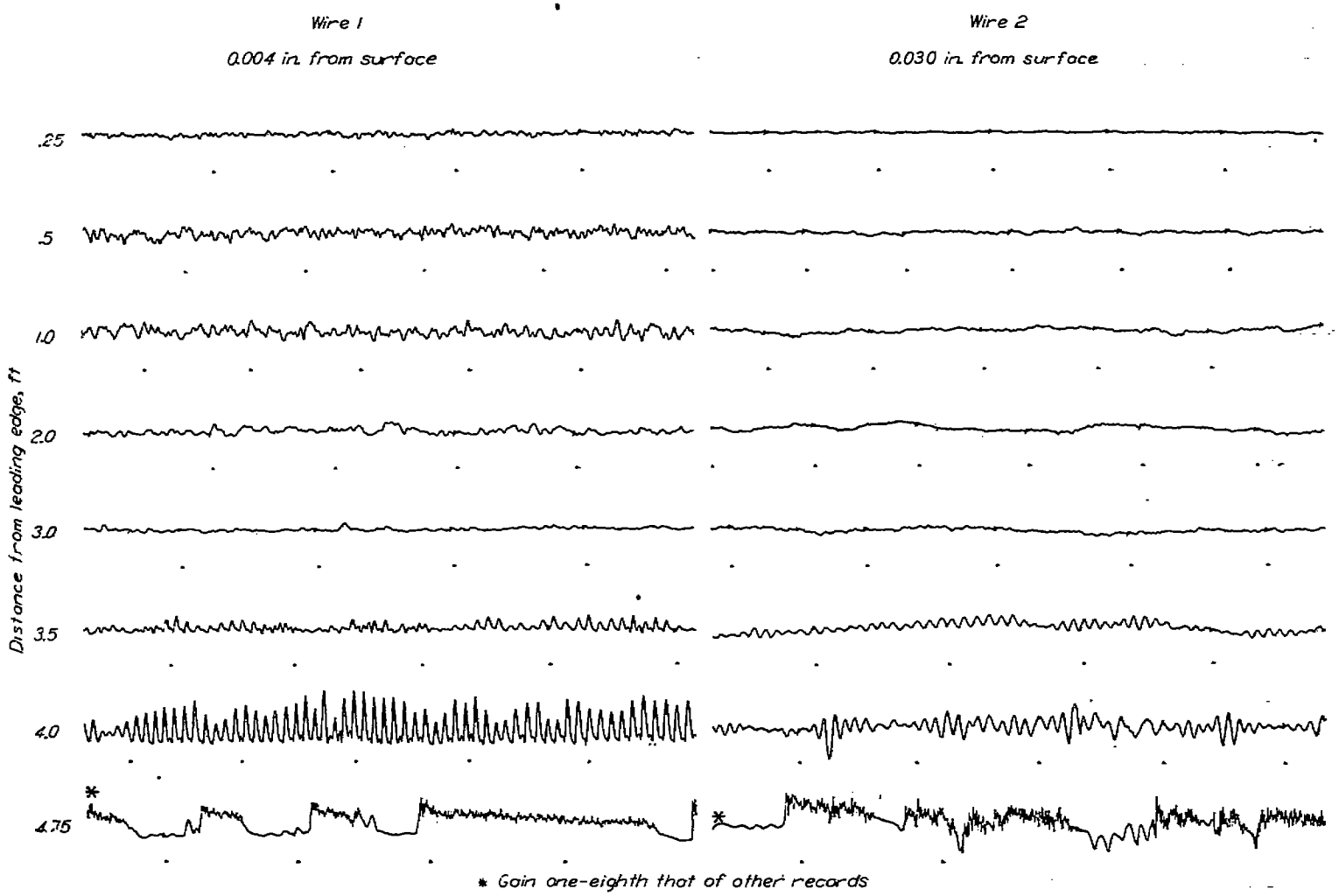

FIGURE 11.—Oscillograms of u-fluctuations showing evidence of frequency doubling near surface. U_1=105 feet per second: time interval between dots, 1/10 second.

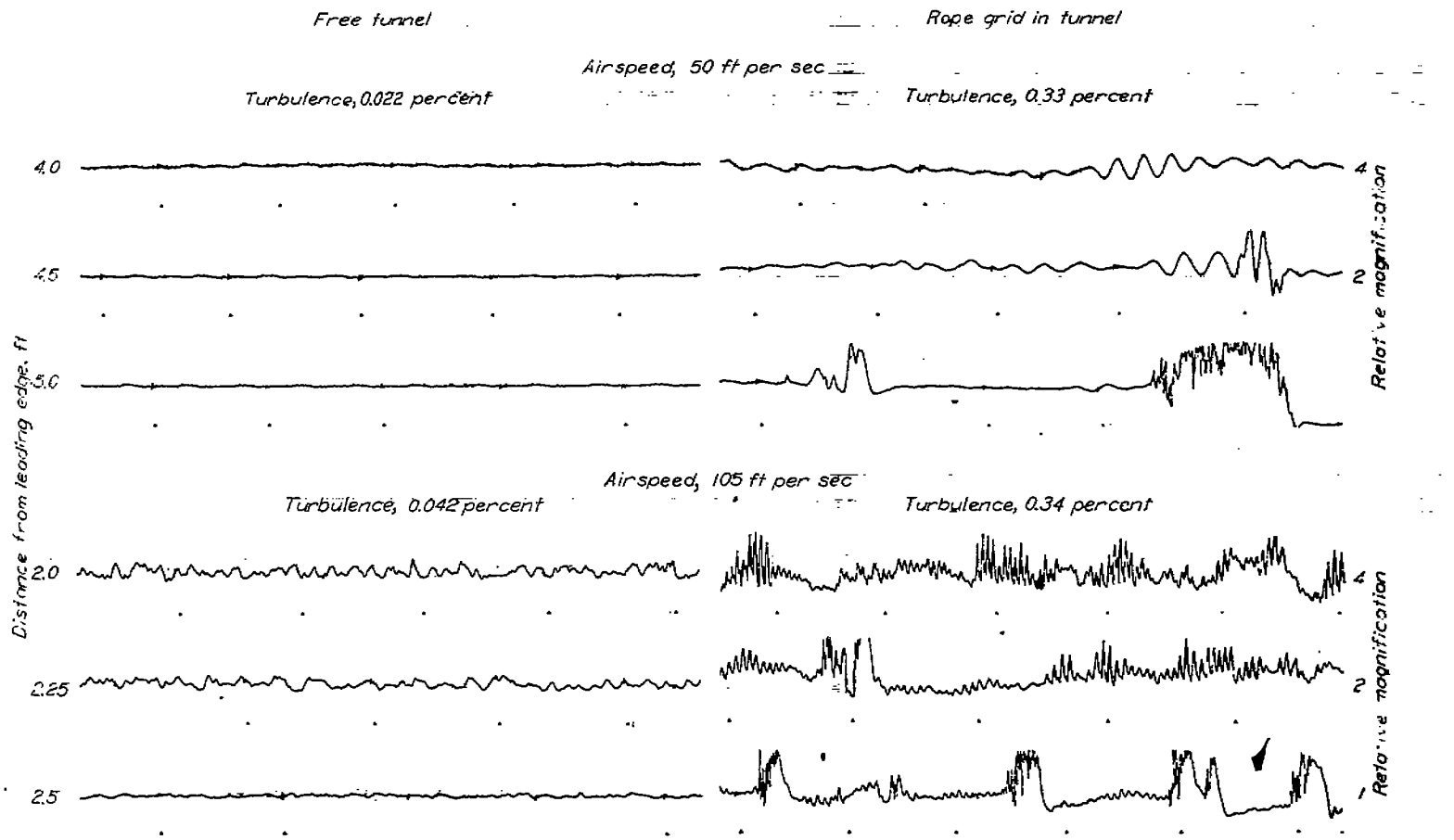

FIGURE 12.—Oscillograms of u-fluctuations showing effect of stream turbulence on boundary-layer oscillations. Distance from surface, 0.004 inch; time interval between dots, 1/50 second.

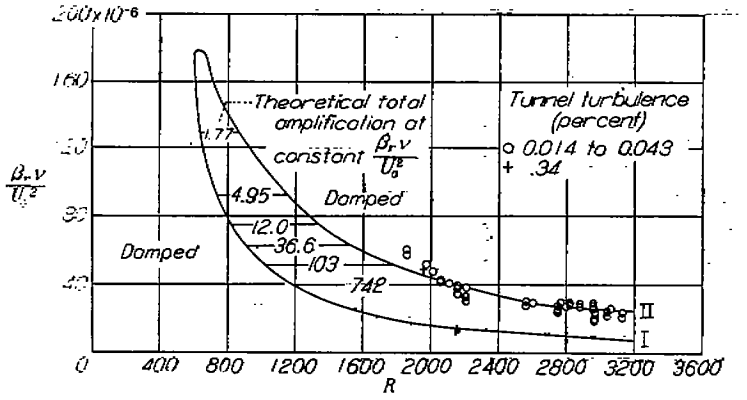

FIGURE 13.—Zone of amplification enclosed by neutral curve according to Schlichting. Theoretical total amplification from branch I to branch II as indicated. Experimental points from frequency of oscillations found on oscillograms. Branches I and II of neutral curve meet R-axis at $R=\infty$.

plification. The oscillations are therefore identified with those produced by instability of the boundary layer.

2. THEORY OF BOUNDARY-LAYER OSCILLATIONS

Evidence has been found of oscillations of rather high purity resulting mostly from random disturbances. The oscillations observed at a fixed point suggest the presence of a traveling wave in the boundary layer. A theoretical answer is sought for the question: How can random disturbances produce a wave that looks closely sinusoidal and has a single predominant frequency?

The superposition of small disturbance velocities on a uniform velocity in one direction presents to a stationary observer the appearance of wave motion. The motion may be sinusoidal or irregular. For simplification, all the disturbance velocity components are assumed to be sinusoidal of the same frequency. In a uniform stream, this motion has the attributes of a traveling wave with a wave velocity equal to the mean velocity of the stream. The amplitude is the disturbance velocity with components u, v, and w, and the pressure involved is the dynamic pressure of the disturbance velocity. This kind of wave is involved in the application of stability theory to the boundary layer. Only two-dimensional motion has so far been successfully treated. In a nonuniform stream, such as a boundary layer, the wave velocity is not known at once but may reasonably be assumed (and can also be proved theoretically) to be less than the maximum velocity of the stream. The characteristics of the wave will depend on the characteristics of the stream, such as the velocity profile of a boundary layer, and on conditions imposed on the mean velocity and on the disturbance velocities at the boundaries. The theory treats the influence of all these conditions and how they determine the wave length, the wave velocity, and the damping or the amplification of the wave.

In general, the disturbances responsible for wave motion in a boundary layer are random in character and the resulting wave motion is irregular. One of the important characteristics of the wave is its ability to maintain itself against the damping action of viscosity or even to grow by absorbing energy from the basic flow. Since this characteristic depends on the frequency, certain component frequencies of an irreg-

ular wave will be damped and others amplified as the wave travels downstream. It will be seen in section VI, 3, that this process accounts for the relatively high purity of the observed boundary-layer oscillations.

Energy considerations alone form the basis of an elementary treatment first used by Osborne Reynolds. According to the Reynolds concept, growth or decay of a disturbance depends on whether energy is transferred to the disturbance by absorption of energy from the basic flow or is extracted from the disturbance by the damping action of viscosity. The flow of energy then determines the stability of the boundary layer under the action of disturbances. Since the kind of disturbance must be specified, this method does not have general applicability. The flow of energy is, however, a fundamental physical concept involved in all theories even though not explicitly stated. As an introduction to the more advanced theories the energy relation will therefore be derived here. The development follows essentially that given by Prandtl in reference 20.

(a) **Basic equations and energy relation.**—In general, only two-dimensional flow with two-dimensional disturbances has been treated successfully in stability theories. The basic flow is assumed to be steady and a function of y only. The basic flow in the boundary layer is then

$$U=f(y)$$

$$V=0$$

The disturbances are a function of time as well as of x and y and are expressed by

$$u=f_1(x,y,t)$$

$$v=f_2(x,y,t)$$

The components of total velocity are therefore $U+u$ and v. Since u and v are assumed to be small, the Navier-Stokes equations become, after squares and products of disturbance velocities and of their differential coefficients are neglected,

$$\frac{\partial u}{\partial t}+U\frac{\partial u}{\partial x}+v\frac{\partial U}{\partial y}=\nu\left(\frac{\partial^2 U}{\partial y^2}+\frac{\partial^2 u}{\partial x^2}+\frac{\partial^2 u}{\partial y^2}\right)-\frac{1}{\rho}\left(\frac{\partial P}{\partial x}+\frac{\partial p}{\partial x}\right) \tag{1}$$

$$\frac{\partial v}{\partial t}+U\frac{\partial v}{\partial x}=\nu\left(\frac{\partial^2 v}{\partial x^2}+\frac{\partial^2 v}{\partial y^2}\right)-\frac{1}{\rho}\left(\frac{\partial P}{\partial y}+\frac{\partial p}{\partial y}\right) \tag{2}$$

where p is the pressure produced by the disturbances and P is the pressure due to the basic flow.

The equation of continuity is

$$\frac{\partial u}{\partial x}+\frac{\partial v}{\partial y}=0 \tag{3}$$

By subtracting from equations (1) and (2), respectively, the corresponding Navier-Stokes equations for $u=v=p=0$, the following two equations are obtained in terms of only the disturbances:

$$\frac{\partial u}{\partial t}+U\frac{\partial u}{\partial x}+v\frac{\partial U}{\partial y}=\nu\left(\frac{\partial^2 u}{\partial x^2}+\frac{\partial^2 u}{\partial y^2}\right)-\frac{1}{\rho}\frac{\partial p}{\partial x} \tag{4}$$

$$\frac{\partial v}{\partial t}+U\frac{\partial v}{\partial x}=\nu\left(\frac{\partial^2 v}{\partial x^2}+\frac{\partial^2 v}{\partial y^2}\right)-\frac{1}{\rho}\frac{\partial p}{\partial y} \tag{5}$$

Equations (4) and (5) are the fundamental hydrodynamic equations for small disturbances on which are based all stability theories herein discussed.

In order to derive an expression for energy balance, equation (4) is multiplied by u and equation (5) by v and the resulting equations added to give the single disturbance equation

$$\rho\left(\frac{\partial}{\partial t}+U\frac{\partial}{\partial x}\right)\left(\frac{u^2+v^2}{2}\right)=$$
$$\mu\left[u\left(\frac{\partial^2 u}{\partial x^2}+\frac{\partial^2 u}{\partial y^2}\right)+v\left(\frac{\partial^2 v}{\partial x^2}+\frac{\partial^2 v}{\partial y^2}\right)\right]-\rho uv\frac{\partial U}{\partial y}-\left(u\frac{\partial p}{\partial x}+v\frac{\partial p}{\partial y}\right) \tag{6}$$

It will be noted that the left-hand member of this equation gives the time rate of change of kinetic energy, due to the disturbances, of a particle moving with the basic flow. Each term on the right-hand side of equation (6) is now integrated over the region containing the disturbance, as explained in detail in reference 20. The resulting expression is

$$\frac{dE}{dt}=-\rho\int\int uv\frac{dU}{dy}\,dx\,dy-\mu\int\int\left(\frac{\partial u}{\partial y}-\frac{\partial v}{\partial x}\right)^2 dx\,dy \tag{7}$$

where dE/dt now represents the time rate of change of kinetic energy, due to the disturbance, of the fluid within the region of integration. The first term on the right-hand side of equation (7) involves the shearing stress ρuv and represents the rate at which energy is absorbed from the basic flow. This energy is added to that already present in the disturbance. The second term on the right-hand side, which is obviously always negative, is the rate of dissipation of the energy of the disturbance by viscosity. The predominance of one effect over the other will determine the net change in the energy of the disturbance.

The first term on the right-hand side of equation (7) has an interesting physical interpretation. First, if u and v differ in phase by 90°, as in the usual wave motion, $\overline{uv}$ will vanish over one complete cycle and no energy can be absorbed from the basic flow. Second, since dU/dy is positive, $\overline{uv}$ must be negative, if the disturbance is to receive energy from the basic flow. These and other conditions are treated in the more advanced theory to be considered next.

(b) **General disturbance equation and solutions.**—Lord Rayleigh (reference 21) appears to have been the first to outline a more general mathematical theory to which numerous investigators have contributed. The mathematical difficulties are so great that the basic velocity profile ($U=f(y)$) was usually approximated by a straight line or segments of straight lines. This imposed serious limitations on the generality of the results. Tietjens (reference 22) was the first to apply Rayleigh's theory to profiles intended to reproduce flow along a wall, but his solution suffered from the serious limitations just mentioned. Important advances

have been made by Tollmien (references 2 and 3) and Schlichting (references 4 to 7), who successfully applied the theory to curved profiles intended to represent actual velocity distributions. Their most complete solutions apply to an approximation of the Blasius distribution. For this distribution Schlichting's work (references 4 and 5) is particularly complete and his results are used here for comparison with experimental results. The following outline of the theory is taken largely from references 4 and 5 with occasional help from reference 2. The physical basis for the theory, the steps in the solution, and the more important results are given here. The mathematical aspects of the problem are discussed in the original references. Even in the original references details of the computations are lacking and checking of results is difficult.

From the basic equations (4) and (5), the pressure terms are eliminated by differentiating equations (4) and (5) with respect to y and x, respectively, and subtracting the second from the first. The result is a linear homogeneous equation in u and v:

$$\frac{\partial^2 u}{\partial y \partial t}+U\frac{\partial^2 u}{\partial x \partial y}+\frac{\partial U}{\partial y}\frac{\partial u}{\partial x}+v\frac{\partial^2 U}{\partial y^2}+\frac{\partial v}{\partial y}\frac{\partial U}{\partial y}-\frac{\partial^2 v}{\partial x \partial t}-\frac{U\partial^2 v}{\partial x^2}=$$
$$\nu\left(\frac{\partial^3 u}{\partial x^2 \partial y}+\frac{\partial^3 u}{\partial y^3}-\frac{\partial^3 v}{\partial x^3}-\frac{\partial^3 v}{\partial y^2 \partial x}\right) \tag{8}$$

The disturbance velocities may be expressed in terms of a stream function ψ, such that

$$\left.\begin{aligned} u&=\frac{\partial \psi}{\partial y}\\ v&=-\frac{\partial \psi}{\partial x}\end{aligned}\right\} \tag{9}$$

Any periodic disturbance may be represented by a Fourier series. Since equation (8) is linear and homogeneous in u and v, its behavior may be investigated by using a single term of the series. This amounts to assuming a periodic disturbance whose stream function has the form:

$$\psi=F(y)\ \exp\ [i(\alpha x-\beta t)]=F(y)\ \exp\ [i\alpha(x-ct)] \tag{10}$$

where $F(y)$ represents the initial amplitude of the stream function which depends only on y, $\alpha=2\pi/\lambda$ where λ is the wave length, and t is the time. Since β and hence c are generally complex quantities, equation (10) may be written

$$\begin{aligned}\psi&=F(y)\ \exp\ \{i[\alpha x-(\beta_r+i\beta_i)t]\}\\ &=F(y)\ \exp\ \{i\alpha[x-(c_r+ic_i)t]\}\end{aligned} \tag{11}$$

where β_r, the real part of β, is the angular velocity or $2\pi f$ (where f is frequency); β_i, the imaginary part of β, is the coefficient of amplification or damping, depending on whether it is positive or negative; and $c_r=\beta_r/\alpha$ is the velocity with which the phase progresses and will be termed simply "wave velocity."

When equation (8) is written in terms of the stream function and substitution is made for ψ in accordance with the second of equations (10), the result is

$$(U-c)(F''-\alpha^2 F)-U''F=\frac{\nu}{i\alpha}(F''''-2\alpha^2 F''+\alpha^4 F) \tag{12}$$

where the primes represent differentiation with respect to y. Equation (12) is a homogeneous linear differential equation of the fourth order with a general solution of the form

$$F=C_1F_1+C_2F_2+C_3F_3+C_4F_4 \tag{13}$$

where F_1, F_2, F_3, and F_4 are the particular solutions and C_1, C_2, C_3, and C_4 are the constants of integration. The form of these particular solutions depends on the basic velocity assumed, that is, on the boundary-layer profile.

A solution of equation (12) was first obtained by Tollmien (reference 2) for a velocity distribution intended to approximate closely a Blasius distribution. He considered the case in which amplification and damping were absent, that is, for real values of β and c, and obtained the so-called "neutral" oscillations. Schlichting (reference 4) repeated Tollmien's calculation and in addition treated the case for small amplification. In a later paper (reference 5), Schlichting determined the distribution of amplitude of neutral oscillations across the boundary layer and investigated the energy balance. Schlichting's work is therefore more complete and more suitable for comparison with experiment.

Both Tollmien and Schlichting approximated a Blasius distribution by a straight line and a parabola as follows:

For $0\leqq\frac{y}{\delta}\leqq 0.175$,

$$\frac{U}{U_0}=1.68\frac{y}{\delta}$$

For $0.175\leqq\frac{y}{\delta}\leqq 1.015$,

$$\frac{U}{U_0}=1-\left(1.015-\frac{y}{\delta}\right)^2$$

For $\frac{y}{\delta}>1.015$,

$$\frac{U}{U_0}=1$$

This gave a sufficiently close approximation to the Blasius distribution of U but was not a sufficiently good approximation for U' and U''. The latter quantities were therefore taken directly from the Blasius solution; only the following terms of the series, which obviously apply to small values of y/δ, were used

$$\frac{U'}{U_0}=1.68\left[1-3.65\left(\frac{y}{\delta}\right)^3\right]$$

and

$$\frac{U''}{U_0}=-18.4\left(\frac{y}{\delta}\right)^2$$

The displacement thickness $\delta^*=\int_0^\delta\left(1-\frac{U}{U_0}\right)dy=0.347\delta$.

Schlichting gives 0.341δ for the integral and this value was used to compute the values of δ in figure 21.

It was assumed that $U=f(y)$ and that $V=0$. This is

equivalent to assuming a nonthickening boundary layer, that is, constant δ, and is the basis for most of the adverse criticism of the theory. In a real boundary layer, δ depends on x, $U=f(x,y)$, and $V\neq 0$; but the dependence of U on x is small compared with the dependence on y, and V is small compared with U.

Since the purpose of the present paper is merely to indicate the method of solving the equation, the solutions will be indicated in general form. The calculations have been carried through to numerical results for only a few velocity profiles.

Equation (12) is not readily solved in its entirety and certain approximations must be made that involve the friction terms on the right-hand side of the equation. The simplest approximation is to neglect the friction terms entirely. In order to justify this, equation (12) is put in a dimensionless form that has the Reynolds number as one of the parameters. When the new independent variable y/δ^* is introduced and $F=U_0\delta^*\phi$, the result is

$$\frac{U-c}{U_0}(\phi''-\alpha^2\delta^{*2}\phi)-\frac{U''\phi}{U_0}=\frac{1}{i\alpha\delta^*R}(\phi''''-2\alpha^2\delta^{*2}\phi''+\alpha^4\delta^{*4}\phi) \tag{14}$$

where the primes now denote differentiation with respect to y/δ^* and R is the Reynolds number. When R is sufficiently large, the right-hand side of equation (14) may be small enough to neglect. The effect of the friction terms is actually negligible for all values of y/δ^* except those near the surface and near a plane,[2] that is also near the surface, where the wave velocity is equal to the local stream velocity. It has been shown by Tollmien (reference 2) that c must always be less than U_0; a point will therefore always be found in the boundary layer where $U=c$. Exclusive of this point and the surface, two particular solutions ϕ_1 and ϕ_2 may be obtained by solving the frictionless equation

$$\frac{U-c}{U_0}(\phi''-\alpha^2\delta^{*2}\phi)-\frac{U''\phi}{U_0}=0 \tag{15}$$

The solutions are expressed as power series developed about y_c, where y_c is the position of the critical point, $U=c$. These solutions are

$$\phi_1=\frac{(y-y_c)}{\delta^*}\left[1+a_2\frac{(y-y_c)}{\delta^*}+a_3\frac{(y-y_c)^2}{\delta^{*2}}+\cdots\right] \tag{16}$$

$$\phi_2=\frac{U''_c}{U'_c}\phi_1\log\frac{(y-y_c)}{\delta^*}+1+b_1\frac{(y-y_c)}{\delta^*}+b_2\frac{(y-y_c)^2}{\delta^{*2}}+\cdots \tag{17}$$

where U''_c and U'_c are the values of U'' and U' at the critical point. While ϕ_1 is regular throughout the whole layer, ϕ_2 possesses a singularity at the critical point and a correction to equation (17) must be found by another approximate solution that takes into account the friction at the critical point. This second approximation to equation (14), valid in the neighborhood of the critical point, results from neglecting all but the largest of the friction terms.

For this purpose a new independent variable η is introduced, defined by

$$\frac{y-y_c}{\delta^*}=\left(\alpha\delta^*R\frac{U'_c}{U_0}\right)^{-1/3}\eta=\epsilon\eta \tag{18}$$

From this it is seen that η is a dimensionless variable which is equal to zero at the critical point $y=y_c$, positive for $y>y_c$, and negative for $y<y_c$. Equation (14) is now written with η as the independent variable for ϕ. Since this equation will be used in the vicinity of $y=y_c$, $\frac{U-c}{U_0}$ can be approximated by $\left(\frac{U'_c}{U_0}\right)\epsilon\eta$ and U'' by U''_c, where the primes again denote differentiation with respect to y/δ^*. The equation becomes

$$i\phi''''+\phi''(\eta-2i\epsilon^2\alpha^2\delta^{*2})-\phi\left(\epsilon\frac{U''_c}{U'_c}+\eta\epsilon^2\alpha^2\delta^{*2}-i\epsilon^4\alpha^4\delta^{*4}\right)=0 \tag{19}$$

where ϕ is differentiated with respect to η. Since ϵ is small, the terms containing ϵ^2 and ϵ^4 are omitted, and equation (19) becomes

$$i\phi''''+\eta\phi''=\epsilon\frac{U''_c}{U'_c}\phi \tag{19a}$$

Equation (19a) contains no singularity at $U=c$ and a solution of this equation at the critical point indicates the form of ϕ_2 to be used when $y-y_c<0$. This form is

$$\phi_2=\frac{U''_c}{U'_c}\phi_1\left(\log\left|\frac{y-y_c}{\delta^*}\right|+i\pi\right)+1-b_1\frac{(y-y_c)}{\delta^*}+b_2\frac{(y-y_c)^2}{\delta^{*2}}+\cdots \tag{17a}$$

By neglecting the term in equation (19a) containing ϵ, the homogeneous equation

$$i\phi''''+\eta\phi''=0 \tag{20}$$

is obtained. The solution of equation (20) contains the two particular solutions ϕ_3 and ϕ_4 which are expressed in terms of Hankel functions as follows:

$$\phi_{3,4}=\int_\infty^\eta d\eta\int_\infty^\eta\eta^{1/2}H^{(1),(2)}_{1/3}\left[\frac{2}{3}(i\eta)^{3/2}\right]d\eta \tag{21}$$

where $H^{(1),(2)}$ are Hankel functions of the first and second kind. Equation (20) is valid all the way to the surface. It is found that ϕ_3 diminishes very rapidly from the surface outward and is therefore important only near the surface. On the other hand, ϕ_4 increases rapidly with y and will not satisfy the requirement that $\phi=0$ at $y=\infty$; hence, C_4 in equation (13) is set equal to zero. The general solution of equation (14) may then be written

$$\phi=C_1\phi_1+C_2\phi_2+C_3\phi_3 \tag{22}$$

[2] Since the theory applies only to a boundary layer of constant thickness, the problem is essentially one-dimensional and this plane is commonly referred to as the critical "point."

(c) **Characteristic-value problem.**—The stability investigation is a characteristic-value problem—that is, one in which the boundary conditions afford sufficient equations between the solutions at the boundaries to determine the values of the parameters for which equation (14) is satisfied, those values being the characteristic values. At $y=\delta$ where $U=U_0=$Constant, the solutions of equation (14) are of the simple form

$$\exp\left(-\alpha\delta^*\frac{y}{\delta^*}\right)$$

$$\exp\left(\alpha\delta^*\frac{y}{\delta^*}\right)$$

The solution with the positive exponent must be ignored as it is infinite at $y=\infty$. As the outer boundary condition, then, $\phi'/\phi=-\alpha\delta^*$. Since ϕ_3 has already disappeared at the outer boundary, the result is

$$C_1(\phi'_{1_\delta}+\alpha\delta^*\phi_{1_\delta})+C_2(\phi'_{2_\delta}+\alpha\delta^*\phi_{2_\delta})=0$$

or

$$C_1\Phi_{1_\delta}+C_2\Phi_{2_\delta}=0 \tag{23}$$

where the sub-subscript δ indicates the solution at the outer boundary and

$$\Phi_{1_\delta}=\phi'_{1_\delta}+\alpha\delta^*\phi_{1_\delta}$$

$$\Phi_{2_\delta}=\phi'_{2_\delta}+\alpha\delta^*\phi_{2_\delta}$$

At the surface, $y=0$ and $\phi=\phi'=0$. The surface boundary conditions are then simply

$$C_1\phi_{1_0}+C_2\phi_{2_0}+C_3\phi_{3_0}=0 \tag{24}$$

$$C_1\phi'_{1_0}+C_2\phi'_{2_0}+C_3\phi'_{3_0}=0 \tag{25}$$

where the sub-subscript 0 denotes solution on the surface.

If ϕ in equation (22) does not vanish identically, the following determinant of the boundary solutions, formed from equations (23), (24), and (25), must equal zero:

$$\begin{vmatrix} \Phi_{1_\delta} & \Phi_{2_\delta} & 0 \\ \phi_{1_0} & \phi_{2_0} & \phi_{3_0} \\ \phi'_{1_0} & \phi'_{2_0} & \phi'_{3_0} \end{vmatrix} =0$$

Solving the determinant gives

$$\frac{\phi_{3_0}}{\phi'_{3_0}}=\frac{\phi_{2_0}\Phi_{1_\delta}-\phi_{1_0}\Phi_{2_\delta}}{\phi_{2_0}\Phi_{1_\delta}-\phi_{1_0}\Phi_{2_\delta}} \tag{26}$$

The left-hand side of equation (26) is a function of η_0, where η_0 is the value of η at the surface. Since by equation (18) η is a function of the parameters $\alpha\delta^*$ and R, the left-hand side of equation (26) is also a function of these parameters. The right-hand side of equation (26) is a function of the parameters $\alpha\delta^*$ and c/U_0. Denoting the left-hand side by G and the right-hand side by E gives

$$G(\eta_0)=E(\alpha\delta^*, c/U_0) \tag{27}$$

Equation (27) is complex and may be separated into two real equations by separating real and imaginary parts. Between these two equations any one of the three unknown parameters, $\alpha\delta^*$, R, and c/U_0, may be eliminated and a relation between the other two found. This has been done by both Tollmien and Schlichting for c real, that is, for oscillations neither amplified nor damped. For this case, equation (27) may be written

$$G_n(\eta_{0n})=E_n(\alpha_n\delta^*, c_r/U_0) \tag{28}$$

where the subscript n denotes neutral oscillations. If c_r is eliminated, a relation between $\alpha\delta^*$ and R is found. This gives the theoretical neutral curve shown in figures 20, 25, and 27. By eliminating $\alpha\delta^*$ the relation between c_r/U_0 and R, shown in figures 26 and 33, is found. Recombination of these quantities results in $\beta_r\nu/U_0^2$, plotted in figures 13, 16, 17, 19, and 24.

The curves just mentioned extend only to the maximum values of R that are of practical interest. Tollmien points out in reference 2 that both branches I and II of these curves approach the R-axis as R approaches infinity. Branches I and II therefore meet at infinity and form a closed curve. Amplification occurs within the region enclosed by the curve. Damping occurs in all other regions.

The values of the parameters are given in table III. The computations were made by a combination of analytical and numerical methods. It may be pointed out that the values obtained by Tollmien and Schlichting show some differences. These are probably due to differences in the details of the computations. Values plotted in the foregoing figures and appearing in table III are Schlichting's results.

TABLE III

THEORETICAL WAVE PARAMETERS FOR NEUTRAL OSCILLATIONS ACCORDING TO SCHLICHTING (REFERENCE 4)

$\frac{c_r}{U_0}$	Branch I			Branch II		
	R	$\alpha\delta^*$	$\frac{\beta_r\nu}{U_0^2}$	R	$\alpha\delta^*$	$\frac{\beta_r\nu}{U_0^2}$
0.200	7200	0.077	2.14×10^{-4}	37,600	0.149	0.79×10^{-4}
.250	3010	.101	8.39	12,000	.188	3.92
.300	1630	.129	25.3	4,640	.223	14.4
.325	1150	.143	40.4	3,290	.238	23.5
.350	893	.159	62.8	2,070	.251	42.4
.375	736	.181	92.2	1,420	.264	69.7
.400	633	.205	129.5	1,020	.274	107.4
.420	606	.239	165.7	713	.273	161.0

Schlichting extended the calculations to include small amplification, applying only in the neighborhood of the neutral curve. The calculations were carried out, not by a direct solution of equation (27) but by a series development starting from the neutral equation (28). Thus $G(\eta_0)$ is found by

$$G(\eta_0)=G(\eta_{0n})+(\eta_0-\eta_{0n})G'(\eta_{0n})+\ \ldots \tag{29}$$

and $E(\alpha\delta^*, c/U_0)$ is found by

$$E(\alpha\delta^*, c/U_0)=E_n(\alpha_n\delta^*, c_r/U_0)+(\alpha-\alpha_n)\left(\frac{\partial E_n}{\partial\alpha}\right)+$$

$$(c-c_r)\left(\frac{\partial E_n}{\partial c}\right)+\ \ldots \tag{30}$$

With the values of G and E given by equations (29) and (30), amplifications were determined near and within the

space enclosed by the neutral curve $\beta_i=0$. Values beyond the range permitted by this method were determined by interpolation, by assuming a cubic equation for β_i at constant R that meets both branches of the neutral curve with the known slope $\frac{\partial\beta_i}{\partial\alpha}$ at these points. Schlichting's diagram showing the theoretical amplification is given in figures 27 and 28. It will be noted that β_i has a maximum near the center of the zone and falls off toward both branches of the neutral curve. In accordance with equation (11), amplification of a disturbance is expressed by

$$\frac{A_2}{A_1}=\exp\int_{t_1}^{t_2}\beta_i dt \tag{31}$$

where A_1 is the amplitude at t_1 and A_2 is the amplitude at t_2. If t_1 is taken on branch I of the neutral curve and t_2 on branch II, the total amplification at constant $\frac{\beta_r\nu}{U_0^2}$ was calculated by Schlichting for several parts of the amplification zone. Schlichting's values are shown in figures 13, 19, and 20. The maximum total amplification up to a given value of x, when disturbances of all frequencies are present, is determined by the equation

$$\frac{A(x)}{A_1}=\exp\left(\max\int_{t_1}^{t(x)}\beta_i dt\right) \tag{32}$$

Schlichting found that the relation between this maximum total amplification and the x-Reynolds number up to an R_x of about 10^6 could be represented by the following interpolation formula:

$$\frac{A(R_x)}{A_1}=0.55\exp\left(0.555\times10^{-5}R_x\right) \tag{33}$$

The solution thus far has determined several characteristics of the wave. For any given value of R and the frequency, it is known whether the wave will be amplified, damped, or neutral. For a given frequency the wave velocity is related to U_0 in a known way and is constant over the cross section of the layer. In like manner the wave length is known in relation to δ^*.

(d) **Distribution of amplitude, correlation, and energy balance.**—The characteristic-value problem gives no information about the relative magnitudes of u and v nor how they are distributed through the boundary layer. How the boundary layer "vibrates," whether as a whole or in parts, remains unknown. This is because the boundary conditions were used to determine only the parameters of the problem and not the constants of integration.

In a second treatment of the theory applied to the flat plate (reference 5), Schlichting completed the investigation by determining the constants in equation (22) for neutral oscillations, that is, for $\beta_i=0$. He was thus able to calculate relative values of u and v and their distribution across the boundary layer. The physically important questions of the correlation between u and v and the energy balance were also answered. The same approximation to the Blasius distribution as used earlier was used here.

Since absolute values of u and v, which obviously depend on the intensity of the impressed disturbance, are of no interest in such a treatment, one of the constants was left undetermined and for convenience was made unity. Thus,

$$C_1=1$$

and, from the boundary conditions expressed by equations (23) to (25), the following values for C_2 and C_3 are obtained:

$$\left.\begin{aligned} C_2&=-\frac{\Phi_{1_\delta}}{\Phi_{2_\delta}}\\ C_3&=\frac{1}{\phi_{3_0}}\left(\frac{\Phi_{1_\delta}}{\Phi_{2_\delta}}\phi_{2_0}-\phi_{1_0}\right)=\frac{1}{\phi'_{3_0}}\left(\frac{\Phi_{1_\delta}}{\Phi_{2_\delta}}\phi'_{2_0}-\phi'_{1_0}\right)\end{aligned}\right\} \tag{34}$$

When the values of the boundary solutions and their derivatives are known, C_2 and C_3 may be determined by equation (34). The general solution ϕ is thereby determined except for an arbitrary intensity factor. From the nature of the particular solution ϕ has real and imaginary parts ϕ_r and ϕ_i, which must be known with their derivatives in order to determine u and v.

The stream function ψ in equation (9) and the first of equations (10) are used to obtain the real parts of $\frac{u}{U_0}$ and $\frac{v}{U_0}$, since $F=U_0\delta^*\phi$, as follows:

$$\left.\begin{aligned}\frac{u}{U_0}&=k\left[\phi_r'\cos(\alpha x-\beta_r t)-\phi_i'\sin(\alpha x-\beta_r t)\right]\\ \frac{v}{U_0}&=k\alpha\left[\phi_r\sin(\alpha x-\beta_r t)+\phi_i\cos(\alpha x-\beta_r t)\right]\end{aligned}\right\} \tag{35}$$

where k is an arbitrary intensity factor. The corresponding root-mean-square values of u and v are

$$\frac{u'}{U_0}=\frac{k}{\sqrt{2}}\sqrt{\phi_r'^2+\phi_i'^2} \tag{36}$$

$$\frac{v'}{U_0}=\frac{k\alpha}{\sqrt{2}}\sqrt{\phi_r^2+\phi_i^2} \tag{37}$$

An expression for the kinetic energy is readily obtained by squaring equations (36) and (37) and adding. The correlation coefficient defined by

$$K=\frac{\overline{uv}}{u'v'}$$

becomes

$$K=\frac{\phi_r'\phi_i-\phi_r\phi_i'}{\sqrt{(\phi_r'^2+\phi_i'^2)(\phi_r^2+\phi_i^2)}} \tag{38}$$

Values of u'/U_0, v'/U_0, and K were calculated by Schlichting for neutral oscillations corresponding to the following two points, one on each branch of the neutral curve:

Branch	R	$\frac{\beta_r\nu}{U_0^2}$	$\alpha\delta^*$	$\frac{c_r}{U_0}$
I	894	62.3×10^{-4}	0.159	0.35
II	2070	42.4	.251	.35

The value of k was chosen to give an average value of $u'/U_0=0.05$ from 0 to δ. Table IV gives the values of u'/U_0, v'/U_0, and K calculated by Schlichting.

It will be seen in table IV that $u'/U_0=0$ at the surface and again at a point near $y/\delta=0.854$ for branch I and near $y/\delta=0.774$ for branch II, after which it again increases for greater y/δ. The values of u'/U_0 are plotted in figure 21,

TABLE IV

THEORETICAL NEUTRAL OSCILLATIONS TAKEN FROM SCHLICHTING (REFERENCE 5)

[For average $u'/U_0=0.05$ from $y/\delta=0$ to $y/\delta=1$]

$\frac{y}{\delta}$	$10\frac{u'}{U_0}$	$100\frac{v'}{U_0}$	K
Branch I; R, 894; $\alpha\delta^*$,* 0.159			
0	0	0	0
.050	.445	.0546	−.032
.090	.647	.158	−.061
.130	.804	.287	−.155
.170	.922	.434	−.169
.209	1.005	.608	−.140
.250	1.016	.795	−.109
.290	1.003	.973	−.064
.370	.854	1.322	−.022
.451	.689	1.605	−.0075
.531	.524	1.820	0
.612	.371	1.984	0
.693	.244	2.098	0
.774	.121	2.170	0
.854	.007	2.193	0
.935	.103	2.180	0
1.015	.211	2.108	0
1.1	.203	2.027	0
1.2	.193	1.935	0
1.3	.185	1.849	0
1.4	.176	1.763	0
1.5	.168	1.681	0
Branch II; R, 2070; $\alpha\delta^*$,* 0.251			
0	0	0	0
.029	.661	.0655	----------
.054	.937	.214	−.121
.074	1.038	.359	−.170
.105	1.108	.595	−.191
.157	1.127	1.028	−.146
.209	1.086	1.445	−.076
.250	.998	1.755	−.010
.290	.906	2.04	.015
.370	.686	2.50	.019
.451	.504	2.87	0
.531	.340	3.10	0
.612	.205	3.26	0
.693	.087	3.35	0
.774	.022	3.37	0
.854	.123	3.33	0
.935	.216	3.22	0
1.015	.305	3.11	0
1.1	.292	2.925	0
1.2	.272	2.72	0
1.3	.252	2.53	0
1.4	.234	2.35	0
1.5	.218	2.18	0

*$\delta^*=0.341\delta$

where the theory is compared with experiment. At the points within the boundary layer where u'/U_0 vanishes, a 180° phase shift occurs in u, meaning that the instantaneous u-component of the oscillation velocity is decreasing on one side of this point while it is increasing on the other. No such phase shift occurs in v. Table IV also shows that correlation does exist between u and v and that $\overline{uv}$ is negative. This means that energy is drawn from the basic flow; and, in accordance with equation (7), this energy must be balanced by the dissipation if the oscillation is to be neither amplified nor damped. Schlichting evaluated both terms in equation (7) by integrating from $x=0$ to $x=\lambda$ and from $y=0$ to $y=\infty$. The net flow of energy was found to be very nearly zero, which indicated that the oscillations were nearly neutral. This result was interpreted as proof of the correctness of the solution to the characteristic-value problem.

A physical explanation of the correlation between u and v is attempted by Prandtl in reference 20. It appears that u and v would differ in phase by 90° and $\overline{uv}$ would vanish in consequence if there were no phase shift in v produced by the viscosity near the critical point. The viscosity is thus responsible for the flow of energy to, as well as from, the disturbance.

(e) Solutions for other conditions.—Tollmien (reference 3) has attempted to generalize the solution sufficiently to include boundary-layer profiles with an inflection point, such as occur with an adverse pressure gradient. For such profiles the sign of U'' changes from positive to negative in passing outward from the surface and, at the inflection point, $U''=0$. The velocity of the neutral wave is shown to be equal to the stream velocity at the inflection point, and an important consequence of this is the absence of a critical point at $U=c$, in the solution of the frictionless equation (15). The conclusion is that profiles with an inflection point are inherently unstable, although neutral oscillations can still exist. These considerations suggest that an adverse pressure gradient is favorable to amplification.

Görtler (reference 23) has investigated the effect of wall curvature on the stability of the boundary layer and found that velocity profiles are unstable if a change of sign occurs in $U''+U'/r$, where r is the radius of curvature of the wall. If an inflection point ($U''=0$) exists, the point where $U''+U'/r=0$ is farther from the surface than the point where $U''=0$ for a convex wall and nearer to the surface for a concave wall. If no inflection point exists, a point where $U''+U'/r=0$ can occur only on a convex wall. It is concluded that convex curvature has a destabilizing effect and that concave curvature has a stabilizing effect.

Solutions for profiles with inflection points are given in references 8 to 10. Rosenbrook (reference 8) investigated the flow through a diverging channel as the channel was towed through still water. Streamlines were made visible by fine particles of aluminum in the water and wavelike motions accompanied by the formation of eddies could be observed as well as the velocity distribution. A solution, following Tollmien in reference 3, was obtained for S-shape velocity profiles approximating those observed. Fair agreement was obtained between the observed and the computed wave lengths. Hollingdale (reference 9) obtained the solution appropriate to the laminar wake formed in one case behind a flat plate and in another behind an airfoil, both towed at low speeds through still water. Oscillating wakes were observed at certain Reynolds numbers and the wave length and the wave velocity were measured. With the appropriate interpretation of theoretical results, fair agreement between calculated and observed wave length and wave velocity was obtained. Savic (reference 10) obtained an exact solution of the frictionless equation (15) for the two-dimensional jet and obtained expressions for the neutral wave length and wave velocity in terms of characteristics of the jet. The theoretical results were compared with observations of wave length and wave velocity made on an acoustically sensitive jet and good agreement was obtained.

Schlichting (reference 6) has determined the effect of centrifugal force by calculating the curves of neutral stability for a boundary layer developed on the inner wall of a rotating cylinder. In reference 7, Schlichting has determined the effect of density gradient on the stability of the boundary layer, using the approximation to the Blasius distribution given in part (b) of this section. Neutral curves outlining the zone of amplification are given. Stability is principally affected by a gravitational field in connection with the density gradient through the boundary layer.

The methods of Tollmien and Schlichting have been applied by Pretsch (reference 24) to the boundary layer on bodies of revolution. The approximate forms of the general disturbance equations from which the four particular solutions are obtained are found to be the same as those for the two-dimensional case; the solutions are therefore the same. The solutions are applied to the known velocity profile at the stagnation point of a sphere and the curve of neutral stability is computed.

3. NATURALLY EXCITED OSCILLATIONS

Naturally excited oscillations are those originating from the amplification of small disturbances naturally present in the stream. These oscillations were treated in section VI, 1, and their frequencies were experimentally obtained and plotted in figure 13. The concept of waves running downstream through the boundary layer has been introduced; the behavior of the oscillations in relation to figure 13 can now be discussed.

One important feature of figure 13 is that the values of amplification coefficient are positive within the zone enclosed by the neutral curve and have values reaching a maximum near the center and falling to zero on each boundary. Outside the zone β_i is negative. All disturbances, whether damped or amplified, travel downstream and therefore in the direction of increasing R since δ^* increases with x. For example, a fixed speed U_0 and a disturbance of frequency such that $\beta_r\nu/U_0^2$ in figure 13 equals 40×10^{-6} are considered. Such a disturbance, if it began at the leading edge of the plate, would be damped as it passed along the boundary layer until it reached a point where R attained the value 1180. From this point to $R=2160$ the disturbance would be amplified and, as it passed beyond this point, would again be damped. If A_1 and A_2 are the amplitudes of the disturbance at the beginning and at the end of the amplification zone, the ratio $A_2/A_1=742$. In other words, the amplitude has increased 742 times while crossing the zone. This is the total amplification given by equation (31). A disturbance of any given frequency will then be most highly amplified when it reaches branch II of the neutral curve.

Figure 8 shows that, in experiment, many frequencies are represented in the initial disturbance. The fact that the observed boundary-layer oscillations contain one predominant frequency must be explained. In order to determine whether theory and experiment are in agreement, the place on the theoretical diagram where the predominant frequency should lie must be found. Instead of traversing the diagram of figure 13 with a wave of a single frequency as in the foregoing illustration, waves of many frequencies, covering a wide range of values of $\beta_r\nu/U_0^2$, are supposed to enter the amplification zone through branch I and undergo amplification at a rate determined by their frequency as they proceed to the value of R at which the observation is made. Initial disturbances are, of course, present in the boundary layer at all values of R and disturbances enter the diagram at all points. Those entering this diagram ahead of branch I are reduced by damping below the prevailing level of the initial disturbances while those entering behind branch I cannot receive full amplification. Disturbances occurring at points corresponding to branch I have the largest initial value and also receive the highest amplification; therefore they are assumed to be the ones whose development should mainly determine the final result at the point of observation. It will be noted that amplification increases without limit as the frequency decreases if no limit is placed on the Reynolds number. The experimental observation, however, is made at a particular value of R and hence of R_x; under this condition it is obvious that one particular value of $\beta_r\nu/U_0^2$ will become more highly amplified than any of the others, this one having the maximum total amplification given by equation (33). This frequency obviously is the predominant one that should be found on the oscillograph records. The remaining question now concerns the position of this most prominent frequency on the diagram, that is, where the experimental points should lie. The problem then becomes one of determining along what line, starting from branch I and running parallel to the R-axis, the total amplification is a maximum up to a given value of R. By taking into account the values of β_i given by Schlichting it was found that, for uniform energy distribution with frequency, this line introduced into the diagram along branch I intersects the prescribed value of R somewhere between the center of the zone and branch II. For more accurate results, both the initial energy distribution and the damping prior to reaching boundary I must be considered. The experimental points should lie inside the zone near branch II. The agreement with theory is not perfect, since many points lie on branch II and outside the zone, but is as good as can be expected from observations of this sort.

The process described here is believed to be one of considerable importance since it is the process by which laminar-boundary-layer oscillations develop from initially random disturbances. In order to develop a pure oscillation, initial disturbances must be so small that a large amount of amplification can occur before transition destroys the laminar layer.

It has been pointed out that the oscillations appear to be three-dimensional. This is to be expected because of the three-dimensional nature of the initial disturbances. The theory, however, concerns two-dimensional oscillations and how this should affect the agreement with experiment is not known.

An apparent discrepancy between figures 7 and 13 must be pointed out. It will be observed in figure 13 that oscillations are indicated for R as high as 3120. This corresponds to an R_x of 3.28×10^6 and, according to figure 7, is in the transition region. The oscillograph records actually showed intermittent turbulence, but it was still possible to read oscillation frequencies from nonturbulent parts of the records. The limits of the transition region are defined statistically by the surface-tube method The discrepancy is therefore only apparent.

In connection with the surface-tube method another effect was noted—namely, that a rise in the surface-tube reading was noted a little ahead of the point where turbulence was indicated by the hot wire. This is believed to be caused by a slightly modified velocity distribution arising from the shearing stress given by $\overline{uv}$ in the oscillations. The lower boundary of the transition region in figure 7 is there-

fore a little too low, but the displacement is small and has no significant effect on the shape of the curve.

VII. ARTIFICIAL EXCITATION OF BOUNDARY-LAYER OSCILLATIONS, ZERO PRESSURE GRADIENT

It was soon realized that a study of boundary-layer oscillations could be carried out to better advantage if they were not caused by accidental disturbances occurring in the wind tunnel but were produced by a controlled disturbance of known amplitude and frequency at some chosen position. This was finally accomplished by the vibrating ribbon discussed in section VII, 3. While a search was being made for devices of various kinds that would accomplish the desired result, effects of sound were tried. Interference from naturally excited oscillations was minimized by making the artificial disturbances much greater than the natural disturbances. The bolting-cloth damping screen was also installed with the six wire screens, but the addition of this screen had no detectable effect on the natural oscillations.

1. SOUND FROM LOUDSPEAKER

The effect of sound intensity on the boundary layer is of interest because sound is an unavoidable source of disturbance both in wind tunnels and in free flight of power-driven aircraft. A 25-watt loudspeaker was accordingly installed in the top of the tunnel at the leading edge of the plate and fed by a variable-frequency oscillator through an amplifier. The intensity and the frequency were controllable.

Interesting effects were easily demonstrated. For example, boundary-layer oscillations could be induced at will merely by choosing the right frequency for a particular position and speed. Transition could be moved 1 or 2 feet ahead of its natural position by the right combination of intensity and frequency. In general, a random noise from the loudspeaker produced similar results, but the effect on the oscillations was not so marked. These were casual observations with no attempt at quantitative measurements.

When quantitative work was attempted, it became apparent that the complicated sound field in the tunnel was a decided draw-back. Figures 14 and 15 show the distribution of sound intensity along the center of the working chamber 3 inches from the plate. Figure 14 shows a standing wave at 48 cycles per second with either a node or a loop at the center of the plate, depending on the type of microphone—that is, crystal microphone, responding to sound pressure, or ribbon microphone, responding to particle velocity. This turned out to be the fundamental frequency of the 12-foot tube formed by the plate and the tunnel walls. The same standing wave could be set up without the loudspeaker when the exciting frequency came from the eight-blade wind-tunnel propeller running at a speed of 360 rpm. Figure 15 shows the distribution at 60 cycles per second. The ribbon microphone and the hot-wire anemometer show nearly the same distribution, as would be expected. These are only a few examples of the sound field and the change in distribution with frequency that serve to complicate any studies with controlled sound intensity.

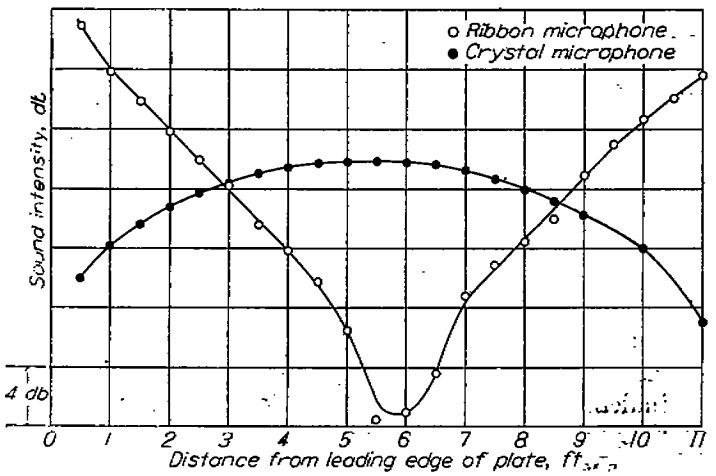

FIGURE 14.—Relative sound intensity from loudspeaker in ceiling of working chamber at leading edge of plate, measured along center 3 inches from plate. U_0=0; frequency, 48 cycles per second.

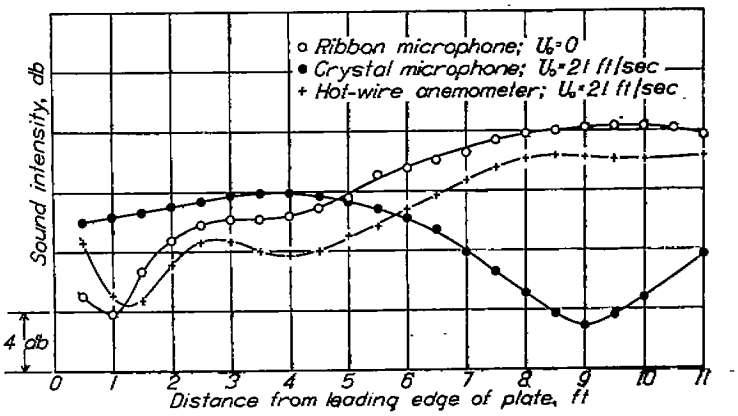

FIGURE 15.—Relative sound intensity from loudspeaker in ceiling of working chamber at leading edge of plate, measured along center 3 inches from plate. Frequency, 60 cycles per second.

When the loudspeaker was used to excite oscillations, two procedures were tried: (1) The sound frequencies that produced oscillations of maximum amplitude at chosen velocities and positions were determined and (2) a sound frequency and position were chosen and the velocity was then varied until the oscillations were a maximum. By use of the sound frequencies read on the oscillator together with the measured U_0 and x, $\beta_r\nu/U_0^2$ and R were calculated and plotted in figure 16. The solid line is again Schlichting's curve of neutral stability enclosing the zone of amplification. Since both procedures amounted to finding the condition for maximum total amplification, the points should lie within the zone near

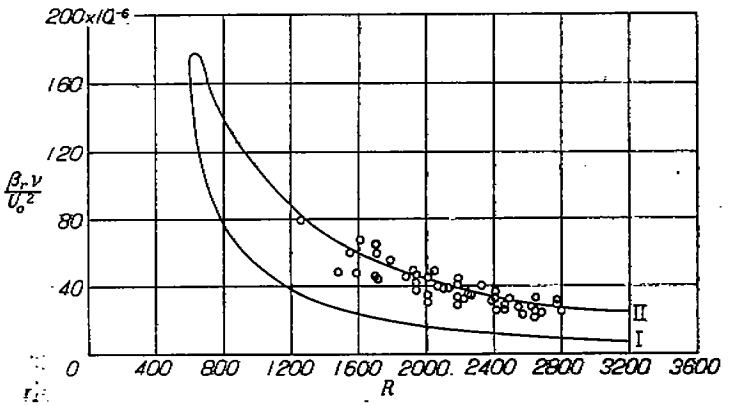

FIGURE 16.—Boundary-layer oscillations excited by loudspeaker. Points show sound frequency giving maximum amplification. Curve outlines theoretical amplification zone. (See fig. 13.)

branch II to be in agreement with theory. In view of the difficulties encountered, the large scattering of the points is not surprising.

Another application of the loud speaker consisted in directly connecting the amplified output of the hot wire to the loudspeaker so that regeneration could occur. Disturbances picked up by the hot wire were thereby fed back as sound, which in turn reinforced the initial disturbance when the proper phase relation existed, causing the system to oscillate. The resulting frequency was read from a variable-frequency oscillator connected to the oscillograph to form Lissajous figures with the hot-wire signal. The frequency of regeneration was determined by the frequency response of the wire, the electrical circuit, the loudspeaker, and the tunnel as a whole, as well as by the preferred boundary-layer frequency. Many frequencies could be found with no wind and only by rejecting these "false" frequencies could results of any reliability be obtained. The results are plotted on the usual diagram in figure 17. Many of the points shown evidently are not related to the boundary-layer oscillations.

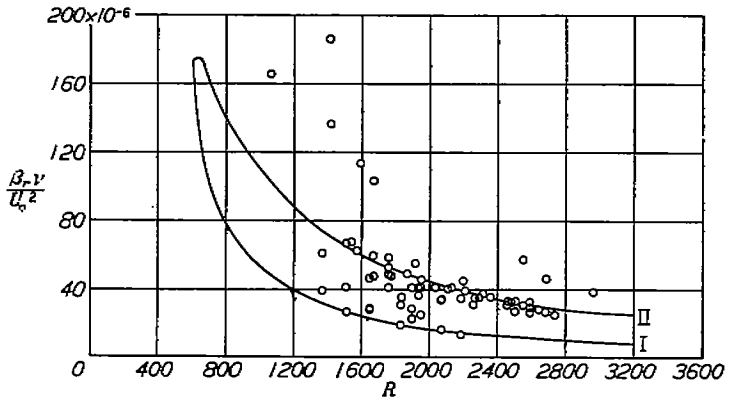

FIGURE 17.—Regeneration frequencies resulting from feedback from hot wire in boundary layer to loudspeaker. Curve outlines theoretical amplification zone. (See fig. 13.)

2. SOUND THROUGH HOLE IN PLATE

A localized disturbance was produced by bringing sound into the boundary layer through a hole in the plate. At a position 18 inches above the center line and 4 feet from the leading edge a ⅛-inch hole was drilled through the plate and on the back was mounted a small headphone from a radio head set. This produced a three-dimensional disturbance emanating from a known location.

A hot wire, mounted on the small sledlike head, was arranged for traversing upstream and downstream at a fixed distance from the surface, usually along a line slightly displaced from the hole. A survey of possible types of measurement showed that the method could be used only for obtaining the type of result shown in figure 18. With the regeneration hook-up, that is, when the amplified output of the wire fed into the headphone, the frequencies of oscillation were determined with the wire at various distances downstream from the hole. The speed was constant during a run. Oscillation of the system occurred most easily for values of U_0 less than 40 feet per second and with the hot wire less than 0.1 inch from the surface. The solid curves of figure 18 show the discontinuous manner in which the frequency varied with the distance. Reversing the connections to the

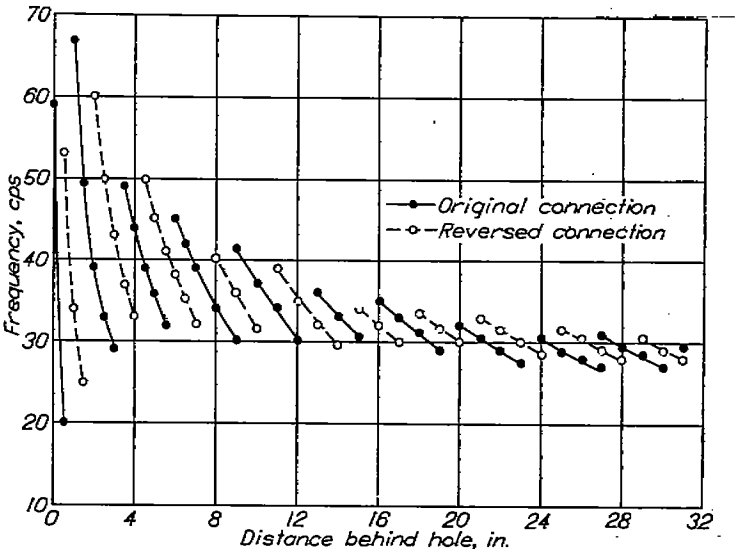

FIGURE 18.—Oscillations excited by sound through hole in plate. Points show regeneration frequencies resulting from feedback from hot wire in boundary layer to headphone. Hot wire moved fore and aft along line 3/16 inch below hole. U_0=23 feet per second.

headphone changed the phase of the input by 180° and gave the results indicated by the broken curves.

The explanation of this sort of performance is that proper phase relations had to exist for regeneration and that the frequency automatically decreased as the distance was increased in order to keep an integral number of waves between the hole and the wire. There existed a preferred frequency band, determined by the characteristics of the wire, electrical and acoustic circuits, and boundary layer. Jumps occurred when another wave between hole and wire was added to keep the frequency as near as possible to the center of the preferred band. The distance between curves of one type along any line of constant frequency is thus the wave length corresponding to that frequency.

It is believed that the frequency band was determined more by the boundary layer than by the rest of the circuit when the wire was far from the hole and that the preferred frequency was that for which amplification was a maximum over the path from hole to wire. The frequency midway between the extremes and as far as possible from the hole was therefore read from sets of curves for different wind velocities like the set in figure 18 and placed on the usual Schlichting diagram. The result is shown in figure 19. The

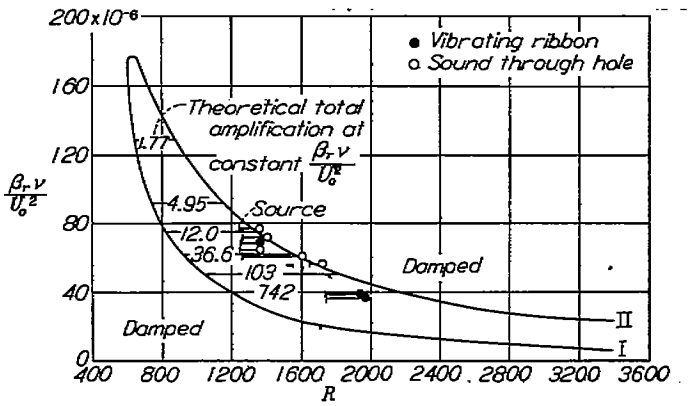

FIGURE 19.—Middle frequencies of regeneration, wire far from hole, taken from curves of type shown in figure 18. Curve outlines theoretical amplification zone. Lines from points show length of amplification path.

path over which amplification could take place is indicated by the horizontal line connected to each point.

Since the wave lengths corresponding to these frequencies were now known, it became possible for the first time to plot the results in terms of $\alpha\delta^*$ and R. The theoretical curve and the experimental results are shown in figure 20. The lines of total amplification for constant $\beta_r\nu/U_0^2$, corresponding to those in figure 19, are known. The paths over which amplification could occur in the experiment are represented as before by lines extending from each point. Figures 19 and 20

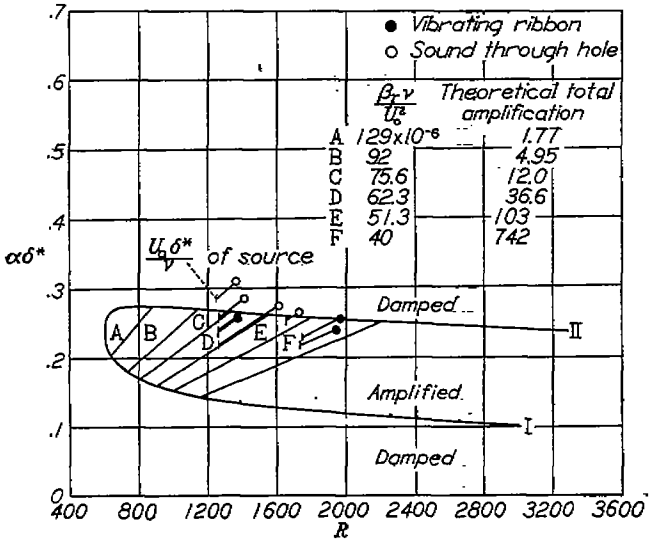

FIGURE 20.—Wave-length diagram showing zone of amplification according to Schlichting. Points show values of $\alpha\delta^*$ for frequencies of figure 19. Lines from points show path of amplification.

generally show the kind of results predicted by theory, if the frequency and wave length are determined mainly by the characteristics of the boundary layer.

3. EXCITATION BY VIBRATING RIBBON

(a) **The ribbon.**—All attempts to excite boundary-layer oscillations by wires vibrating in the boundary layer failed because the disturbance of the eddying wake from the vibration of wires large enough to affect the layer produced early transition. Flat strips outside the layer suffered from self-induced flutter and also had troublesome wakes that carried with them fluctuating pressure fields far downstream. A thin flat ribbon of phosphor bronze, placed edgewise to the flow in the boundary layer and only a few thousandths of an inch from the surface, was finally found capable of oscillating the boundary layer but produced no detectable effect when not vibrating. The ribbon was driven in and out from the surface by passing through it a small current of the desired frequency in the presence of a strong magnetic field from an electromagnet on the opposite side of the plate.

Several ribbons were tried to find the best width, distance from surface, and length of vibrating span. All ribbons were 0.002 inch thick. Widths ranged from $\frac{1}{16}$ to $\frac{1}{4}$ inch; distances from surface, from 0.006 to 0.015 inch; and vibrating segments, from 6 to 12 inches. None of these factors appeared to affect the performance to any noticeable extent. A certain amount of tension was necessary for stability. When it was desired to place the resonant frequency above the working range, high tension was necessary.

After this preliminary work, a ribbon 0.1 inch wide and 3 feet long was installed 4 feet from the leading edge of the plate. At a distance of 6 inches from each side of the center line of the plate, two strips of Scotch cellulose tape were laid on the surface for insulation and spacing. Another strip of tape was then laid on the ribbon to hold it firmly in contact with the tape on the plate, except for the segment 12 inches long at the center. Rubber bands at the ends supplied the tension. The 12-inch segment at the center was 0.006 inch from the surface and was free to vibrate under the action of the current and the magnetic field. Examinations with a microscope showed that the ribbon vibrated to and from the surface in a single loop. The same oscillator and amplifier that had been used for the loudspeaker were found to furnish ample power for driving the ribbon. Different positions for the ribbon were chosen to cover a large range of Reynolds number but the method of attachment was always the same. Distance from the surface varied somewhat for different installations.

(b) **Procedure.**—Two hot wires, one 0.010 inch and the other 0.110 inch from the surface, both sensitive only to u, were mounted on the small sledlike head and arranged for sliding upstream and downstream along the center line of the plate with the distance of the wires from the surface fixed. The fluctuations introduced into the boundary layer could be picked up by either hot wire. The wave form showed some distortion for an inch or so behind the ribbon but in general became nearly sinusoidal at greater distances. Frequencies amplified by the boundary layer showed increasing amplitude with increasing distance from the ribbon, while those damped showed decreasing amplitude. For much of the working region the oscillations could probably be regarded as two-dimensional but no attempt was made to verify this assumption.

Just as for the loudspeaker and the headphone behind the hole in the plate, the system could be made to oscillate by connecting the amplified output of the hot wire to the ribbon. Curves like those shown in figure 18 were obtained and, from them, three points plotted in each of figures 19 and 20 were obtained. Since the ribbon could be used for applications that were believed to be more important, very little work was done with the regeneration hook-up.

The wave length was determined in the following simple manner: The input to the ribbon from the oscillator was connected to one pair of plates in the cathode-ray oscillograph and the output from the wire was connected to the other pair. A stationary Lissajous figure consisting of a single closed loop was obtained since the frequencies of both input and output were the same. As the spacing between ribbon and hot wire was changed this figure changed from a straight line to an ellipse, then to a circle, again to an ellipse, and finally to a straight line inclined 90° to the first line. This indicated that the phase between input to the ribbon and output from the wire had changed by 180° and that the change in spacing between wire and ribbon was ½ wave length. With the oscillograph serving as the indicator, wave-length measurements were thus reduced to a measurement of the distance moved by the hot wire. The wave velocity was then obtained by multiplying the wave length by the frequency of the oscillations.

Determinations of amplification and damping were carried out by setting the ribbon into vibration at an arbitrary fixed amplitude and reading the mean-square hot-wire output voltage as the wire was moved away from the ribbon. The results obtained are given in section VII, 3 (d). The distribution across the boundary layer was determined by traversing normal to the surface at some fixed distance behind the ribbon with a single hot wire sensitive to u mounted on the traversing apparatus described in section III, 7.

During the course of the work frequencies ranging from 10 to 260 cycles per second were used.

(c) **Distribution of amplitude across boundary layer.**—Since a theoretical distribution of amplitude across the boundary layer has been given by Schlichting (see sec. VI, 2 (d), and table IV), the actual distribution is of interest as a test of agreement between theory and experiment. Traverses across the boundary layer were therefore made with a hot wire downstream from the ribbon with frequency, air velocity, and distance from the leading edge of the plate chosen to conform to the conditions for which the theoretical calculations were made. These conditions correspond to oscillations on the neutral curve specified as follows:

Conditions required by theory						
Branch		R		$\frac{\beta_{cr}\nu}{U_0^2}$		
I II		894 2070		62.3×10^{-6} 42.4		
Experimental conditions						
Branch	R	$\frac{\beta_{cr}\nu}{U_0^2}$	x (ft)		U_0 (fps)	Frequency (cps)
			Ribbon [1]	Wire		
I II	902 2080	61.4×10^{-6} 40.6	0.75 5.00	1.09 5.33	41.8 46.0	103 82

[1] Ribbon about 0.009 in. from surface.

The distributions are given in figure 21 with amplitude expressed in terms of u'/U_0. The solid curves show the theoretical distribution and the broken curves through the points show the observed distribution. In both cases the traverses were made 4 inches behind the ribbon. The vibrational amplitude of the ribbon was set arbitrarily and about the same for branches I and II. The smaller values of u'/U_0 in branch II result from the smaller effect of the ribbon on the thicker boundary layer. Since the theoretical values given by Schlichting were based on an arbitrary average amplitude of $u'/U_0=0.05$ from $y=0$ to $y=\delta$, Schlichting's values were reduced to give the average found by experiment; that is, areas under the theoretical curves were made equal to areas under the experimental curves from $y=0$ to $y=\delta$.

Although the general agreement between theory and experiment is good, perhaps the most striking confirmation of the theory is the 180° phase shift occurring at $y/\delta=0.7$. On moving outward from the surface all oscillations disappeared at this point and farther out they reappeared but with phase opposite to those that had disappeared. This phenomenon

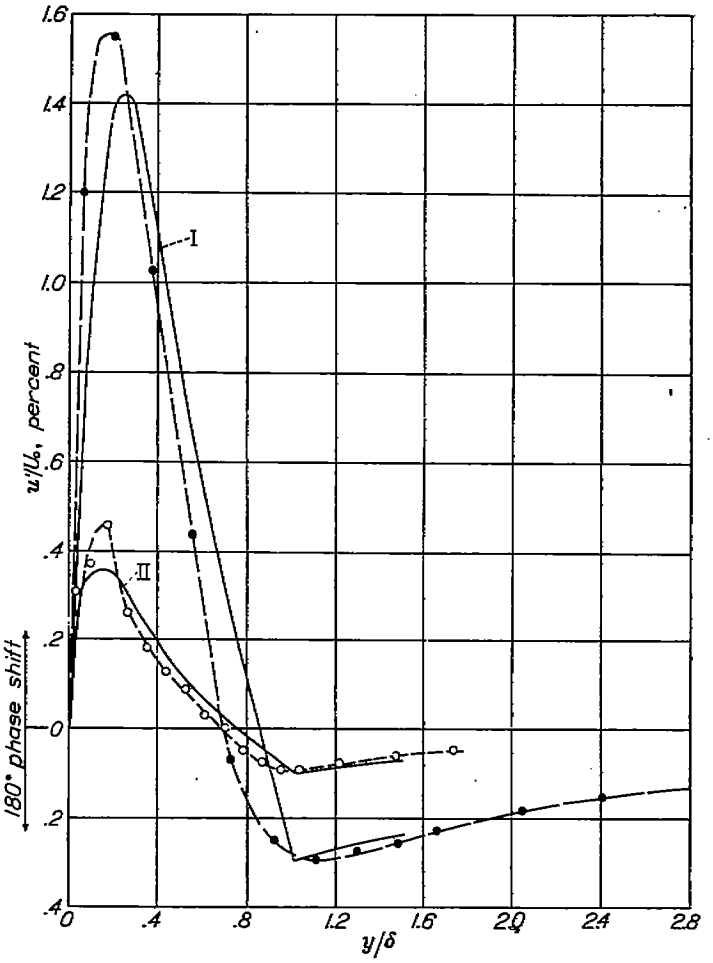

FIGURE 21.—Distribution of amplitude of oscillations across boundary layer. Solid curves are theoretical according to Schlichting. Broken curves are experimental.

is shown in a more striking manner by the oscillograms in figure 22. The pairs of traces are simultaneous records of oscillations picked up by two wires, one of which was at a fixed distance of 0.055 inch from the surface (lower trace) and the other at varying distances, beginning at 0.080 inch (upper trace). The simultaneous records were made possible by an electronic switch that impressed the separately amplified voltages of the two wires on the oscillograph, alternately and in rapid succession. The switching from one to the other accounts for the dotted appearance of the trace. The waves are in phase for the first four records; the amplitude of the upper wave decreases with each succeeding record to zero in the fifth. Beginning with the sixth, an oscillation reappears in the upper trace but 180° out of phase with that in the lower trace. The oscillations in these records lie near the center of the amplification zone at $R=1720$.

The type of distribution shown in figure 21, including the phase reversal, was found for amplified, damped, and neutral frequencies and for oscillations as close as 1 inch behind the ribbon and as far downstream as the oscillations remained free from transition disturbances. The fact that the main features of the distribution were found 1 inch behind the ribbon shows that the forced oscillations in the boundary layer very soon reach a steady state.

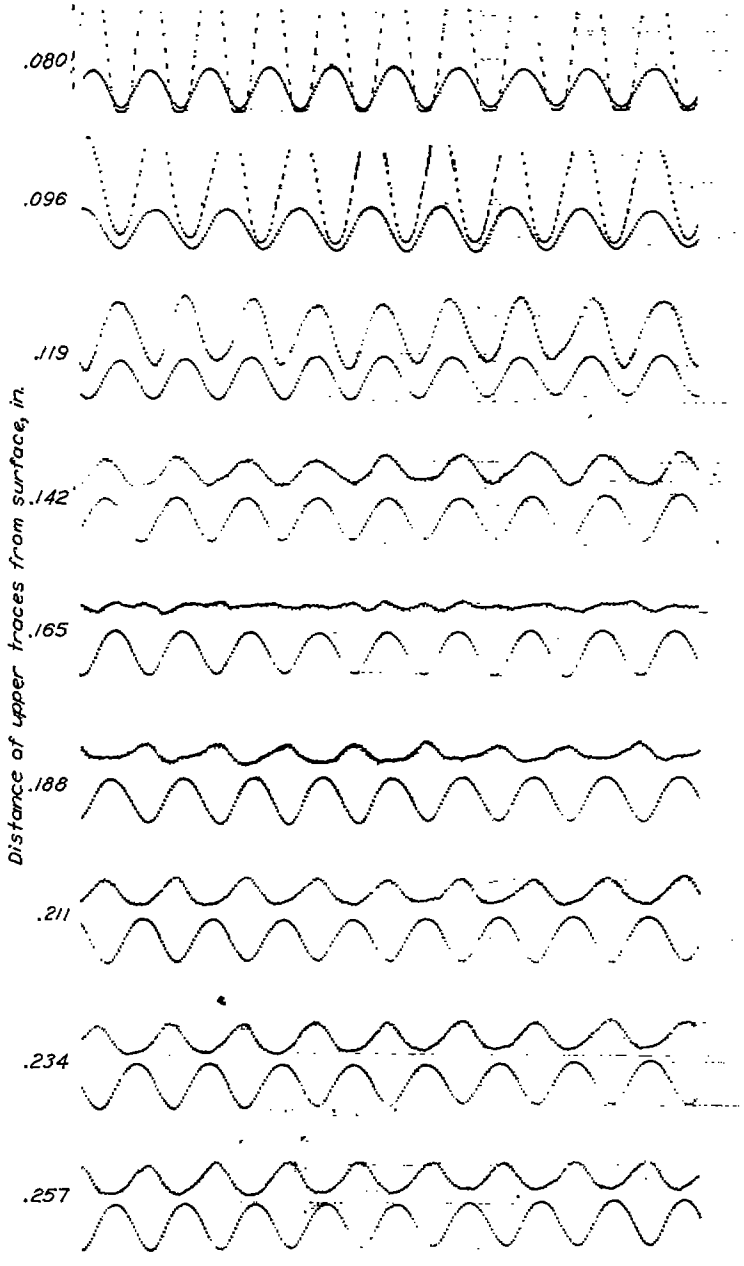

FIGURE 22.—Oscillograms showing phase reversal in u-component of oscillations excited by vibrating ribbon. Simultaneous records from two hot wires located 1 foot downstream from ribbon. Lower trace, hot wire 0.055 inch from surface; upper trace, hot wire at various distances from surface; ribbon 3 feet from leading edge of plate; frequency, 70 cycles per second; U_0=42 feet per second.

(d) Amplification and damping.—When the wire was kept at a fixed distance from the surface and moved downstream from the ribbon, the amplitude of the forced oscillation either increased, decreased, or remained the same, depending on the frequency, the velocity, and the Reynolds number. The amount of the change with distance could be determined by reading the mean-square value of the fluctuating voltage across the wire on the output meter of the turbulence amplifier. In order to eliminate as far as possible the extraneous disturbances introduced by turbulence and by the noise of the tunnel, the signal from the wire was passed through an electrical filter, which was tuned in each case to pass only a 5-cycle band around the frequency being measured. The results of a typical run with the ribbon at the 4-foot position are shown in figure 23. In this figure x_0

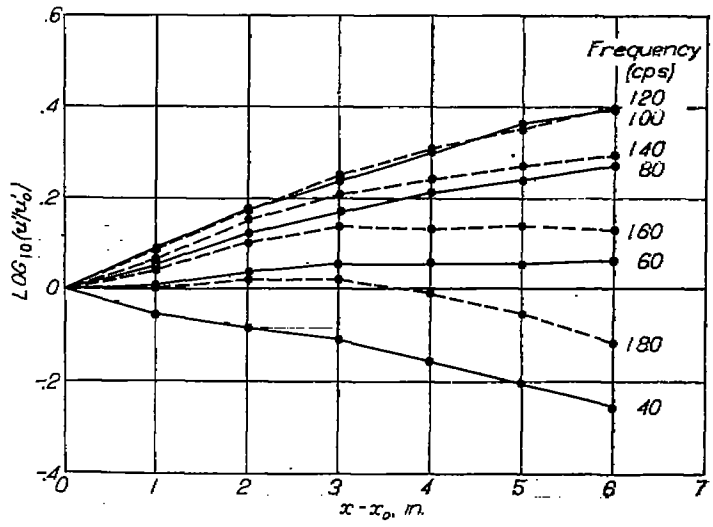

FIGURE 23.—Growth and decay of u-component of oscillations produced by vibrating ribbon 4 feet from leading edge of plate. x_0, 2 inches downstream from ribbon; U_0=64 feet per second.

denotes a position 2 inches downstream from the ribbon. The ratio u'/u_0' is the square root of the meter reading at x divided by the square root of the meter reading at x_0.

According to equation (31)

$$\frac{u'}{u_0'}=\exp\int_{t(x_0)}^{t(x)}\beta_t\,dt$$

or

$$2.3\log_{10}\frac{u'}{u_0'}=\int_{t(x_0)}^{t(x)}\beta_t\,dt$$

Differentiating with respect to t and using the relation $dx/dt=c_r$, where c_r is the wave velocity, give

$$\beta_t=2.3\,c_r\frac{d\left(\log_{10}\frac{u'}{u_0'}\right)}{dx} \tag{39}$$

The wave velocity is obtained by multiplying the measured wave length by the frequency. If the changes in u'/u_0' with distance shown in figure 23 are truly effects of amplification and damping, the slopes of the curves in this figure serve to determine β_t.

Before these slopes can be used with confidence, effects introduced by the thickening of the layer with increasing x and effects from possible changes in the distribution across the layer also with x must be investigated. Errors can arise from these sources because of the experimental procedure—namely, the determination of growth or decay of amplitude by varying the distance between the ribbon and the wire while keeping the wire at a fixed distance from the surface. From the evidence in section VII, 3 (c), changes in the distribution are small and can cause but little error; however, the increase of δ with x may give rise to an apparent amplification or damping, depending on the position of the wire in the layer. In all cases in which data on amplification and damping were obtained, the wire was in the rising part of the distribution, that is, values of y/δ below those for maximum u'/U_0 in figure 21. Consequently, the increasing δ with increasing x introduced an apparent damping, which caused all observed amplification to be less than the true

value and all observed damping to be too great. If it is assumed that the inner part of the distribution curve is a straight line passing through the origin, the magnitude of the error in β_i calculated from equation (39) by use of observed slopes is $\frac{1}{2}\frac{c_r}{x}$. Any curvature in the distribution curve like that shown between zero and the peak value of u'/U_0 in figure 21 lessens the error. Since $\frac{1}{2}\frac{c_r}{x}$ therefore represents an upper limit and since its value turned out to be about the order of the random deviation in results, β_i was calculated by equation (39) with the use of the experimentally determined slopes without correction.

In figure 23 the curve for 40 cycles per second shows damping throughout. As the frequency is increased amplification takes place, reaches a maximum at 120 cycles per second, and then decreases until 180 cycles per second again shows damping. In the range of Reynolds number represented by this range in x, all frequencies below about 50 and above 180 cycles per second are damped, while a band of amplified frequencies lies in between.

Of considerable interest are the frequencies for which there is neither amplification nor damping and the corresponding values of R. This amounts to finding points of zero slope on curves like those shown in figure 23. Such points were obtained from a number of runs at various wind speeds with the ribbon at the 4-foot position and again with the ribbon 9 inches from the leading edge. Values of $\beta_r\nu/U_0^2$ and the corresponding values of R were computed and plotted in figure 24. The solid curve is again Schlichting's neutral curve and the broken curves are those defined by the experimentally determined points. The agreement is very satisfactory, except for points above $\beta_r\nu/U_0^2=200\times10^{-6}$.

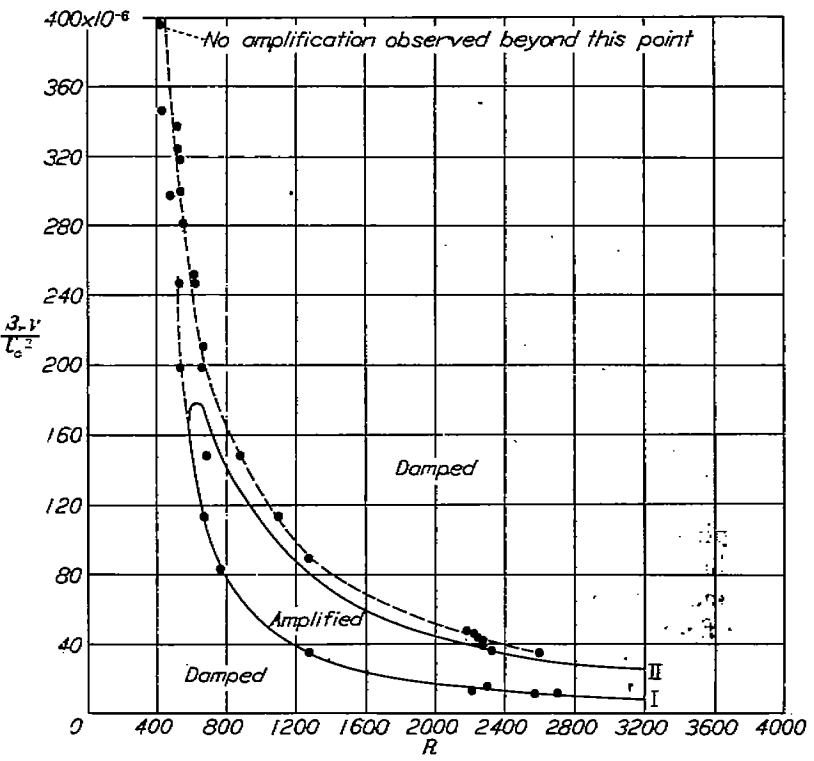

FIGURE 24.—Frequency of neutral oscillations excited in boundary layer by vibrating ribbon. Solid curve is neutral curve according to Schlichting. Broken curves are neutral curves defined by experimental points.

By use of the measured wave lengths, $\alpha\delta^*$ was calculated for the neutral frequencies and the results were plotted on the wave-length diagram shown in figure 25. Schlichting's

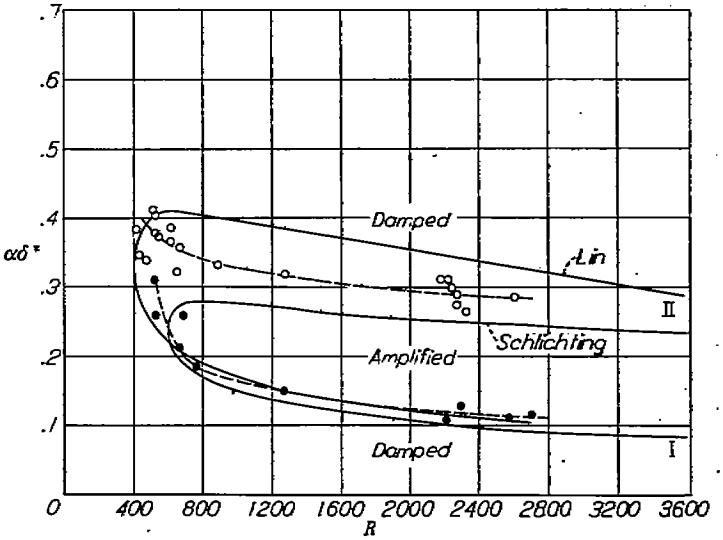

FIGURE 25.—Wave length of neutral oscillations excited in boundary layer by vibrating ribbon. Theoretical neutral curves shown solid, neutral curves defined by experimental points shown broken. Closed circles, branch I. Open circles, branch II.

neutral curve is shown by a solid line and the broken curves are those defined by the experimental points.[3] Open circles denote points on branch II, and closed circles, points on branch I.

Still another type of representation involving both frequency and wave length is the diagram c_r/U_0 and R in figure 26. The points and the broken curves show the wave velocities found for the neutral oscillations. The solid curve is Schlichting's theoretical curve.

It is again pointed out that both branches of the theoretical curves in figures 24 to 26 meet the R-axis at $R=\infty$

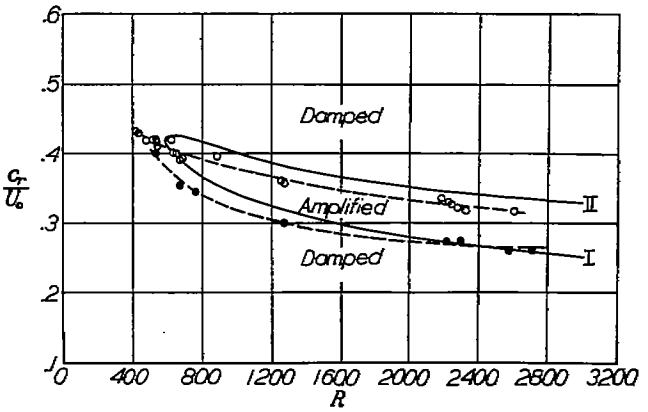

FIGURE 26.—Wave velocity of neutral oscillations excited in boundary layer by vibrating ribbon. Solid curve is neutral curve according to Schlichting. Broken curves are neutral curves defined by experimental points. Closed circles, branch I. Open circles, branch II.

and thus extend beyond the region indicated. Transition prevented experimental determinations above $R=2800$.

The wave-length diagram is repeated in figure 27 and this time shows, in addition to the theoretical neutral curve, the

[3] The theoretical neutral curve given by C. C. Lin has been added in figure 25. Lin's curve was not available when this work was originally written. The curve is taken from C. C. Lin, "On the Stability of Two-Dimensional Parallel Flows," Quart. Appl. Math., vol. III, no. 2, July 1945, pp. 117–142; no. 3, Oct. 1945, pp. 218–234; and no. 4, Jan. 1946, pp. 277–301.

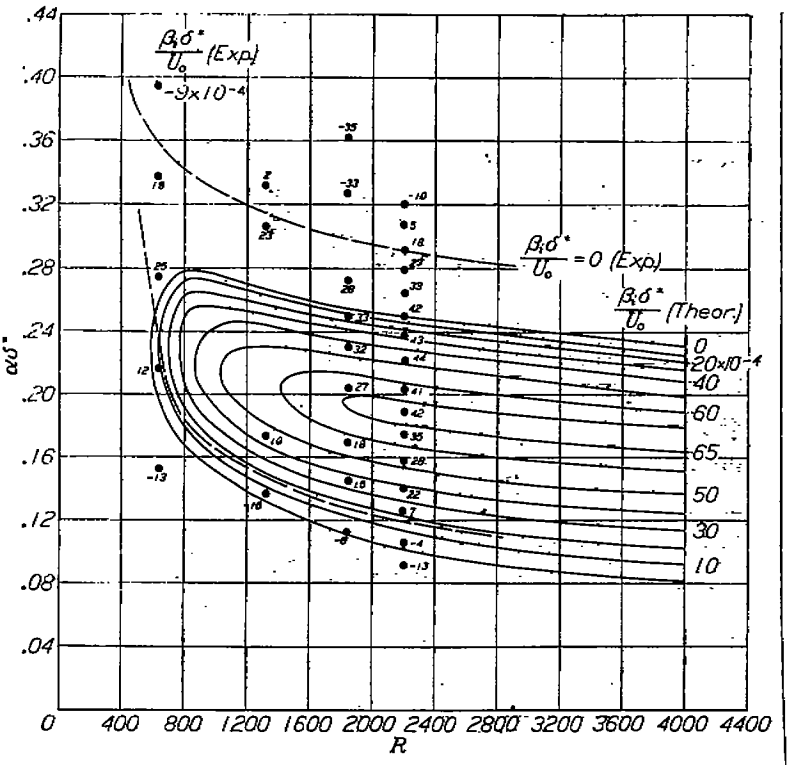

FIGURE 27.—Contours of equal amplification according to Schlichting. Values of $\beta_i\delta^*/U_0$ (all values to be multiplied by 10^{-4}) opposite points are amplifications determined by experiment. Faired experimental contour of zero amplification shown by broken curves.

curves of equal amplification within the zone. These contours were copied directly from a figure given by Schlichting in reference 4. The broken curves are defined by the neutral points, which are not shown in this figure. The points with the values opposite (all to be multiplied by 10^{-4}) are the observed values of $\beta_i\delta^*/U_0$ obtained from values of the slopes other than zero. Negative values signify damping.

The distribution across the amplification zone at particular values of R is shown in figure 28. The theoretical curves, drawn solid, are plotted from values read from Schlichting's figure in reference 4. The broken curves are drawn through the experimental points.

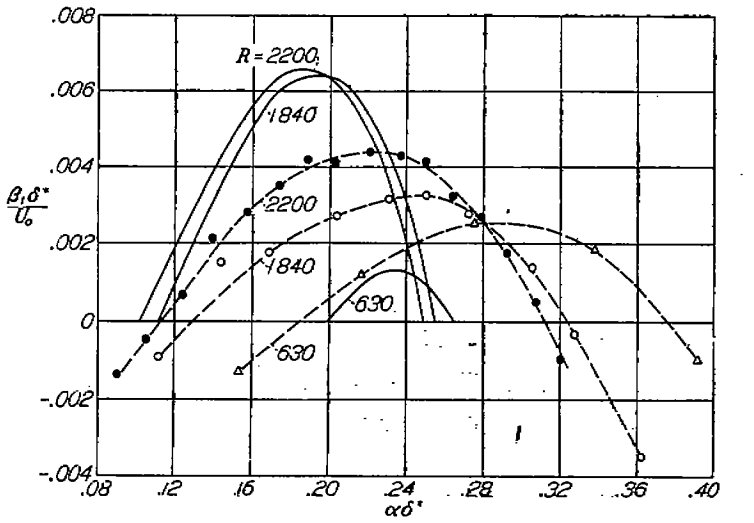

FIGURE 28.—Distribution of amplification across zones of figure 27. Solid curves are theoretical. Broken curves are experimental.

The comparison between theory and experiment given in figures 24 to 28 shows, on the whole, better agreement than might be expected when it is considered that at the outset the very existence of such phenomena had not been proved. The observed amplification shown in figures 27 and 28 is generally less than the theoretical, but it will be recalled that the theoretical calculation yielded accurate values only near the neutral curve. In the neighborhood of the low Reynolds number limit the experimental inaccuracies are large because of the small amplification and damping. The maximum values of $\beta_r\nu/U_0^2$, $\alpha\delta^*$, and c_r/U_0 and the minimum value of R for which amplification can occur as determined approximately by experiment are compared with the theoretical limits in the following table:

	Experiment (approx.)	Theory	
		Schlichting	Tollmien
R	450	575	420
$\frac{\beta_r\nu}{U_0^2}$	400×10^{-6}	178×10^{-6}	----------
$\alpha\delta^*$	0.4	0.278	0.367
$\frac{c_r}{U_0}$	0.43	About 0.42	0.425

Tollmien's limiting values, on the whole, agree better with experiment than Schlichting's values. A comparison of the experimental results in figure 25 with Tollmien's diagram of $\alpha\delta^*$ plotted against $\log_{10} R$ in reference 2 shows better agreement in general than with the corresponding diagram given by Schlichting in figure 25. In spite of this, Schlichting's results were used because they were more complete than Tollmien's.

VIII. EFFECT OF PRESSURE GRADIENT ON BOUNDARY-LAYER OSCILLATIONS

Figure 29, obtained in connection with the earlier work presented in section VI, 1, shows the effect of pressure gradient on naturally excited oscillations. The pressure distribution along a part of the plate is shown to the left in this figure. The reduction of amplitude in the region of falling pressure is very marked. Accelerated growth of amplitude is evident in the region of rising pressure. It was accordingly inferred that negative pressure gradients decreased amplification (or increased damping) of the oscillations while positive gradients increased amplification. A quantitative investigation of this effect was therefore undertaken with oscillations forced on the boundary layer by the vibrating ribbon.

When the ribbon was in the 3-foot position, the regular procedure of measuring amplifications and damping and of mapping the neutral curves was carried out for pressure distributions B, C, D, and E shown in figure 30. The corresponding pressure gradients are given in table V.

In figure 30, q_x is the dynamic pressure at any distance x from the leading edge while q_0 is a convenient reference pressure. Curve A shows one of the distributions for the condition generally termed "zero pressure gradient." This condition was obtained by giving sufficient divergence to the

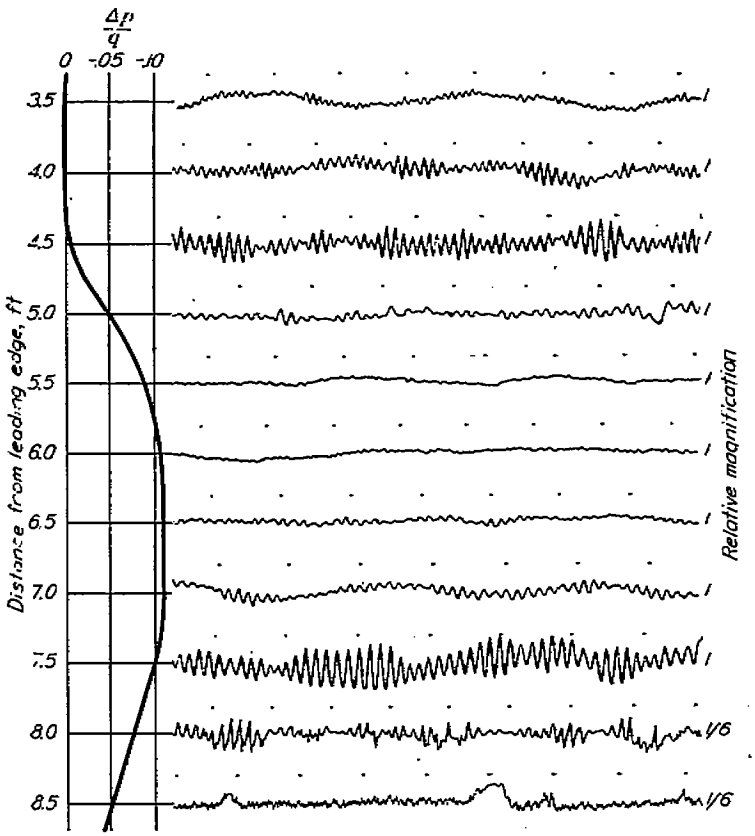

FIGURE 29.—Oscillograms of u-fluctuations showing effect of pressure gradient on boundary-layer oscillations. Distance from surface, 0.021 inch; U_0=95 feet per second; time interval between dots, 1/30 second.

TABLE V

PRESSURE GRADIENTS $\left(\frac{1}{q_1}\frac{\Delta P}{\Delta x}\right)^1$

[q_1, dynamic pressure outside boundary layer at 3.33 ft from leading edge of plate; P, pressure near surface at distance x from leading edge]

Distribution	Average gradient from 1 to 6 feet (percent)	Local gradient (percent)
A	−0.11	−0.78 from 4 to 5 ft
B	1.62	2.48 from 3 to 3.67 ft
C	−2.38	−1.36 from 3 to 3.67 ft
D	----------	12.0 from 3 to 3.67 ft
E	----------	−9.8 from 3 to 3.67 ft

[1] Note that pressure gradient and dynamic pressure gradient have opposite signs. (See fig. 30.)

adjustable side walls of the working chamber to overcome the normal pressure drop. The shape of the curve in the first 6 inches was determined by the flow around the leading edge of the plate and hence could be changed but little by the setting of the walls. The walls also had little effect on the small local variations, since these were found to be produced by slight waviness of the surface. Curve A is thus a condition of zero gradient only when the length of the interval and the end points are properly chosen. With a pressure distribution given by curve A, the experimental values of velocity distribution and δ^* were in good agreement with the Blasius values; hence, the approximation to zero gradient is probably sufficiently good.

Curve B, which shows the pressure rising along the plate, was obtained by giving the walls their greatest possible divergence. Curve C, which shows the pressure falling, was

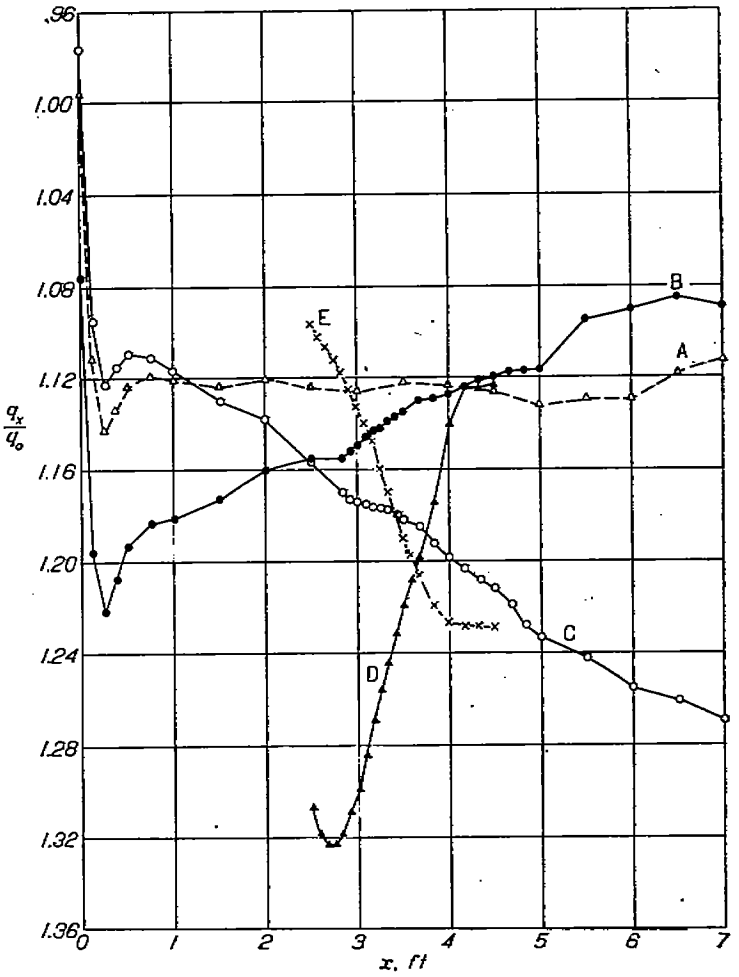

FIGURE 30.—Dynamic pressure distribution along plate outside boundary layer.

obtained with the walls forming a converging passage. The steep positive gradient shown by curve D was produced by a vertical airfoil placed 10 inches from the side of the plate running from the floor to the ceiling of the tunnel, and the steep negative gradient of curve E was produced by blocking the stream with a plywood panel ¾ inch thick and 28 inches wide extending from the floor to the ceiling placed parallel to and 10 inches from the plate.

The results obtained on the effect of pressure gradient are given in figures 31 to 34 for distributions B and C and will be discussed in detail later in this section. Corresponding figures for distributions D and E could not be obtained because of the large effect of these gradients on the oscillations. With the large gradients, the general impression given by observing the oscillations was that amplification always occurred in gradient D regardless of the frequency and Reynolds number, while damping always occurred in gradient E; however, this statement must be somewhat qualified. For example, in E fluctuations of all frequencies were damped for values of R up to 2600, which was the highest value obtainable with the ribbon at the 3-foot position. It is quite possible that a zone of amplification lay beyond the range of the experiment. In the case of gradient D, the investigation had to be restricted to low Reynolds numbers because of the occurrence of transition. The few observations made here indicated a possible low limit of

Reynolds number below which damping occurred, but the results are in doubt because of a possible scale effect on the airfoil used to produce the pressure gradient. The pressure rise may have been lessened by laminar separation on the airfoil at the low velocities and the positive gradient may have become less than that given by D. Accurate measurement of pressure distribution at the low velocities was difficult.

Before presenting the results for the two small gradients B and C, attention must be called to the effect of pressure gradient on δ^*. Since δ^* enters into certain dimensionless quantities used in plotting the results, its actual value must be known for each case. The value of δ^* was measured only for distribution B and the result was

$$\frac{\text{Observed } \delta^*}{\text{Blasius } \delta^*} = 1.09 \text{ at } x = 3.33 \text{ feet}$$

For distribution C, δ^* was estimated by the aid of the Kármán-Pohlhausen method by assuming a linear pressure distribution. The validity of the method was tested by making a similar calculation for B and obtaining good agreement with the measured δ^*. The estimated result for C was

$$\frac{\text{Calculated } \delta^*}{\text{Blasius } \delta^*} = 0.93 \text{ at } x = 3.33 \text{ feet}$$

The values of δ^* for the Blasius distribution were multiplied by these factors to give the value of δ^* pertaining to gradients B and C.

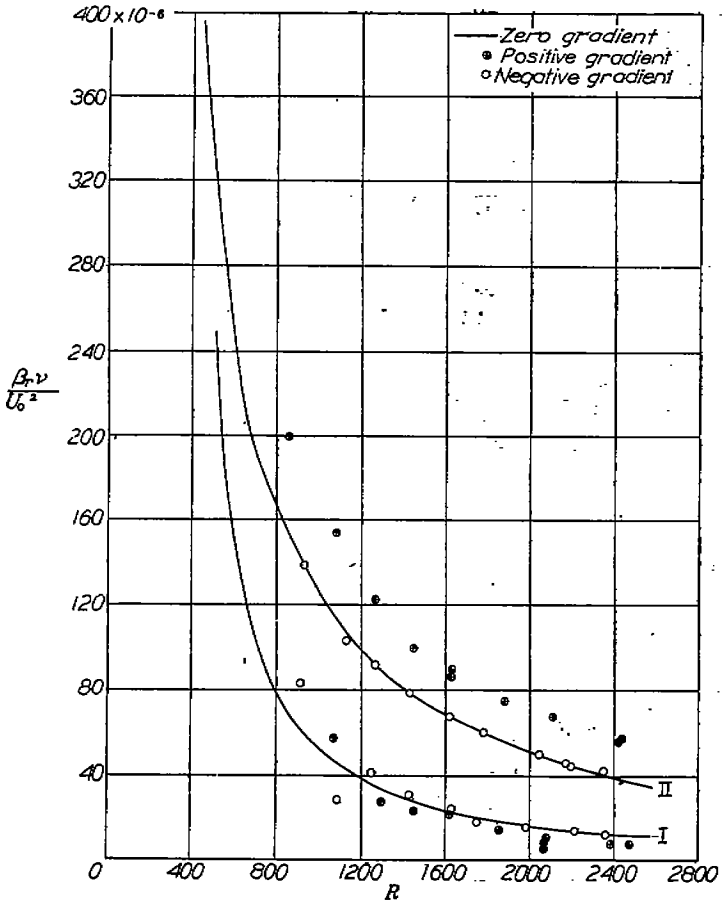

FIGURE 31.—Frequency diagram of neutral oscillations. Experimental curve for zero pressure gradient shown without points. Positive gradient from distribution B and negative gradient from distribution C of table V.

Figure 31 is the much-used frequency diagram showing the results for zero, positive, and negative gradients of distributions A, B, and C, respectively. The solid curve is the same as the broken curve of figure 24 for zero gradient, shown here without the experimental points. The points for negative gradient lie close to this curve; the points for positive gradient generally lie outside the zone of amplification for zero gradient. The positive gradient has therefore widened the amplification zone as expected. Contrary to expectation, the negative gradient failed to reduce the size of the zone. No observations were made below $R=800$.

Since wave lengths of the oscillations were measured, the data for these same frequencies are given in a wave-length diagram (fig. 32) and a wave-velocity diagram (fig. 33). It

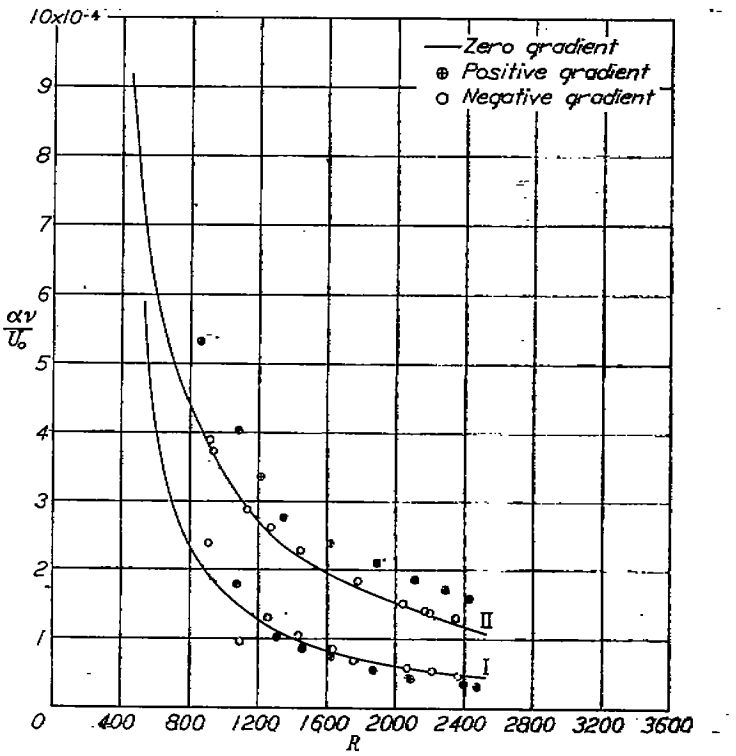

FIGURE 32.—Wave-length diagram of neutral oscillations. Experimental curve for zero pressure gradient shown without points. Positive gradient from distribution B and negative gradient from distribution C of table V.

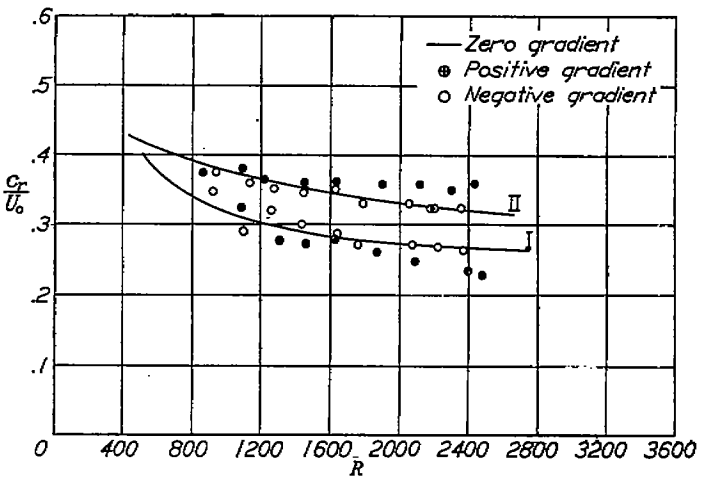

FIGURE 33.—Wave-velocity diagram of neutral oscillations. Experimental curve for zero pressure gradient shown without points. Positive gradient from distribution B and negative gradient from distribution C of table V.

will be noted that figure 32 is unlike the usual wave-length diagram (for example, fig. 25) in that the ordinate is now $\alpha\nu/U_0$ instead of $\alpha\delta^*$. This change was made in order to eliminate δ^* from one of the coordinates and thereby to restrict errors occurring in the estimated value of δ^* with pressure gradient to the Reynolds number coordinate. The new ordinate is simply $\alpha\delta^*$ divided by the Reynolds number, that is,

$$\frac{\alpha\delta^*}{\frac{U_0\delta^*}{\nu}}=\frac{\alpha\nu}{U_0}$$

In both figures 32 and 33, the solid curves are the experimentally determined neutral curves for zero gradient with the experimental points omitted.

Figures 32 and 33, like figure 31, show an effect of the positive gradient but little or no effect of the negative gradient. These figure show only the neutral points and so merely define the boundaries of the amplification zone. The effect of pressure gradient on the amplification within the zone is demonstrated in figure 34. This figure, which is similar to figure 28 except that zones are from the frequency diagram instead of the wave-length diagram, shows the distribution of amplification coefficient $\left(\text{actually } \frac{\beta_i\delta^*}{U_0}\right)$ across the zones of figures 31 at certain fixed values of the Reynolds number. The positive and negative pressure gradients signify as before pressure distributions B and C, respectively. For comparison, the experimental curves for zero gradient are given as solid lines. The comparison is best made between pairs of curves having Reynolds numbers most nearly alike. Since $\frac{\beta_i\delta^*}{U_0}$ increases with Reynolds number (see fig. 27), the difference between $R=1840$ for zero gradient and $R=1810$ for negative gradient may account for the reduced amplification with negative gradient. The failure to show conclusively an effect of the small negative gradient may be due in part to the small local value of the gradient shown in table V. The difference between $R=2200$ for zero gradient and $R=2050$ for positive gradient is significant, since $R=2050$ for zero gradient would lie below $R=2200$.

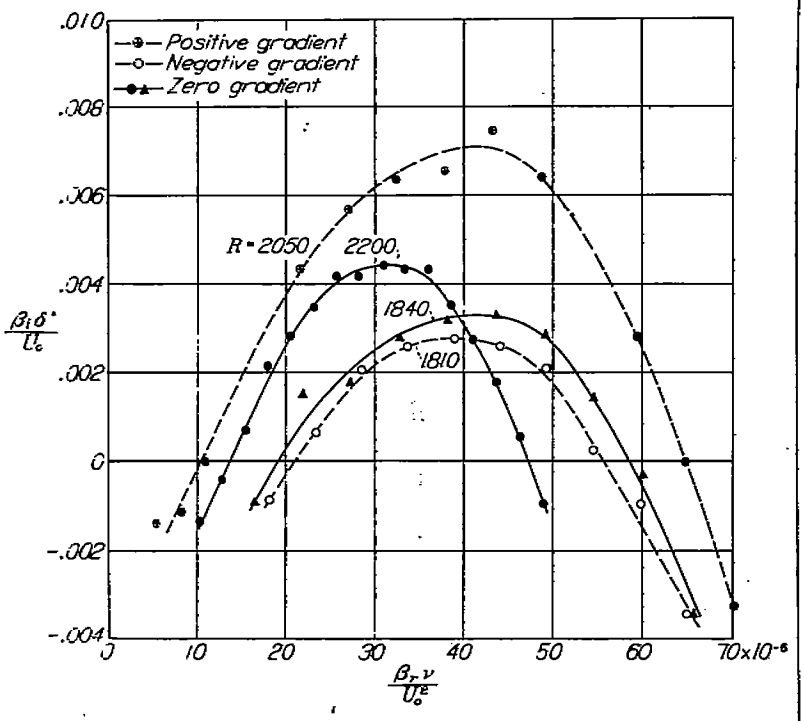

FIGURE 34.—Distribution of amplification across zones of figure 31, showing effect of pressure gradient. Positive gradient from pressure distribution B and negative gradient from distribution C of table V.

IX. TRANSITION FROM OSCILLATIONS TO TURBULENCE, ZERO PRESSURE GRADIENT

The distinguishing feature of transition with low stream turbulence is the occurrence of boundary-layer oscillations that grow until the layer becomes turbulent. Under such conditions, transition to turbulent flow is simply transition from a particular type of oscillatory motion to turbulent motion. The oscillations are now understood and the final step in an understanding of the origin of turbulence involves an investigation of this transition process.

Although transition in highly disturbed flow does not fall into this category, the two are similar in that both have to do with the effect of a disturbance large enough to bring about turbulent flow. The effect, however, depends on the type of the disturbance as well as its magnitude; and, as has been shown, an amplified disturbance does not have the random character of an initially large disturbance. Transition from an amplified disturbance promises to be of considerable importance in modern low-turbulence wind tunnels and in the atmosphere.

The vibrating ribbon to produce oscillations and the hot-wire apparatus to examine their development were suitable tools for the investigation of transition. The ribbon was placed at the 3-foot position and two hot wires at different distances from the surface were arranged for traversing parallel to the plate through the transition region. The Reynolds number was always chosen so that the undisturbed boundary layer (ribbon not vibrating) was laminar at the hot wires. Representative samples of the results obtained are shown in figures 35 to 37.

Figure 35 shows what happens at a fixed point 2.5 feet downstream from the ribbon as the vibrational amplitude of the ribbon is varied. The pairs of traces show simultaneously the response of the two wires. The values of gain control setting on driving amplifier are roughly proportional to ribbon amplitude. The amplitude of the waves on the traces cannot be quantitatively related to fluctuations of velocity because the sensitivity of the wires was unknown. The sensitivities of the two wires were different, and so comparison of amplitudes at inner and outer wires was impossible. It is known, however, that velocity increases produce upward displacement of the traces and that velocity decreases produce downward displacement. The direction of time in this figure is from left to right.

This figure shows that the boundary layer at a given point can be changed from laminar to turbulent by varying ribbon amplitude and shows qualitatively the progressive nature of the change. Examination of successive pairs of traces indi-

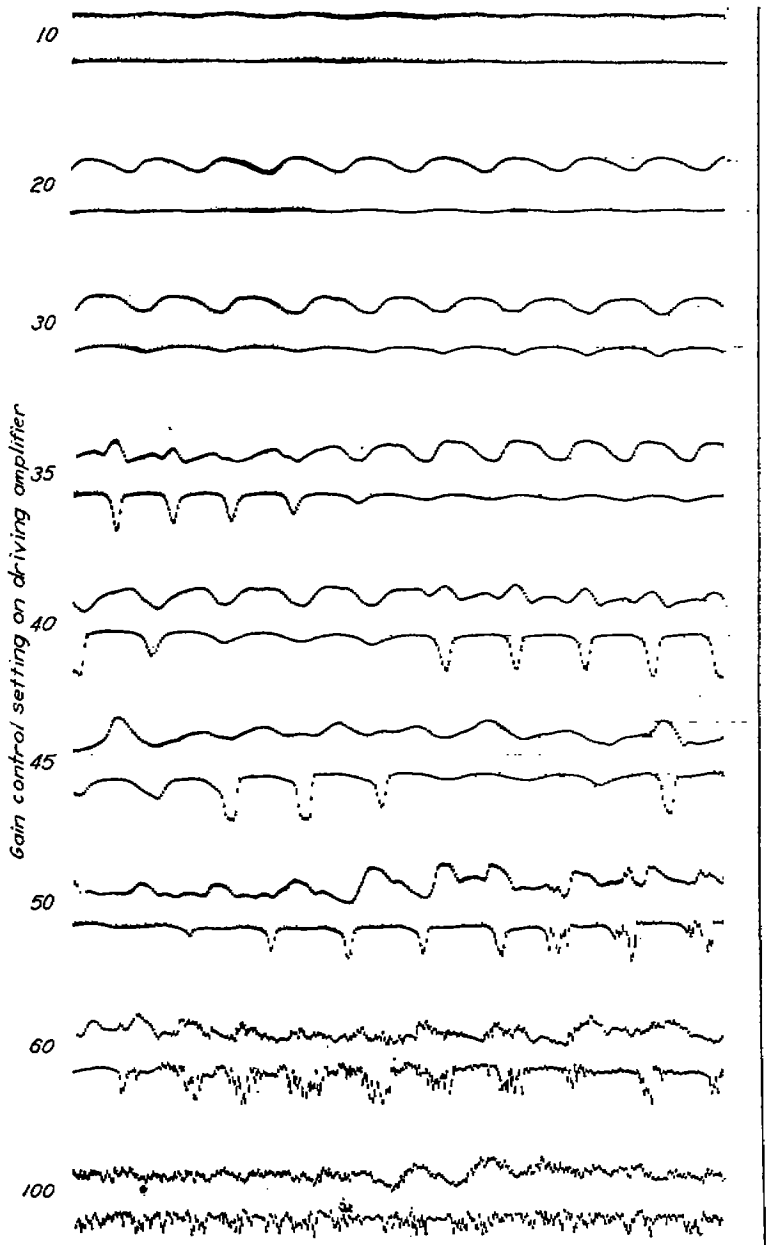

FIGURE 35.—Oscillograms of u-fluctuations showing development of turbulence from oscillations produced by vibrating ribbon. Simultaneous records from two hot wires located 2.5 feet downstream from ribbon. Upper trace, hot wire 0.014 inch from surface; lower trace, hot wire 0.114 inch from surface; ribbon 3 feet from leading edge of plate; frequency, 70 cycles per second; U_0=50 feet per second.

cates that fairly regular waves first make their appearance, being first in phase at the two wires and later in the fifth and sixth records, in and out of phase in random fashion as the amplitude increases. The distances from the surface are such that an in-phase condition would be expected from the distribution in figure 21. A growing distortion of the waves then appears until, in the seventh record, bursts of high-frequency fluctuations occur. The latter, identified by the jagged appearance of the trace, are bursts of turbulence. The final record shows the completely turbulent state. The dotted character of the traces, due to the electronic switch, obliterates details of rapid fluctuations. A similar succession of changes is shown in figures 36 and 37.

In figure 36 simultaneous records are again shown, this time from two wires on the same mounting moved downstream from the ribbon while the amplitude of the ribbon

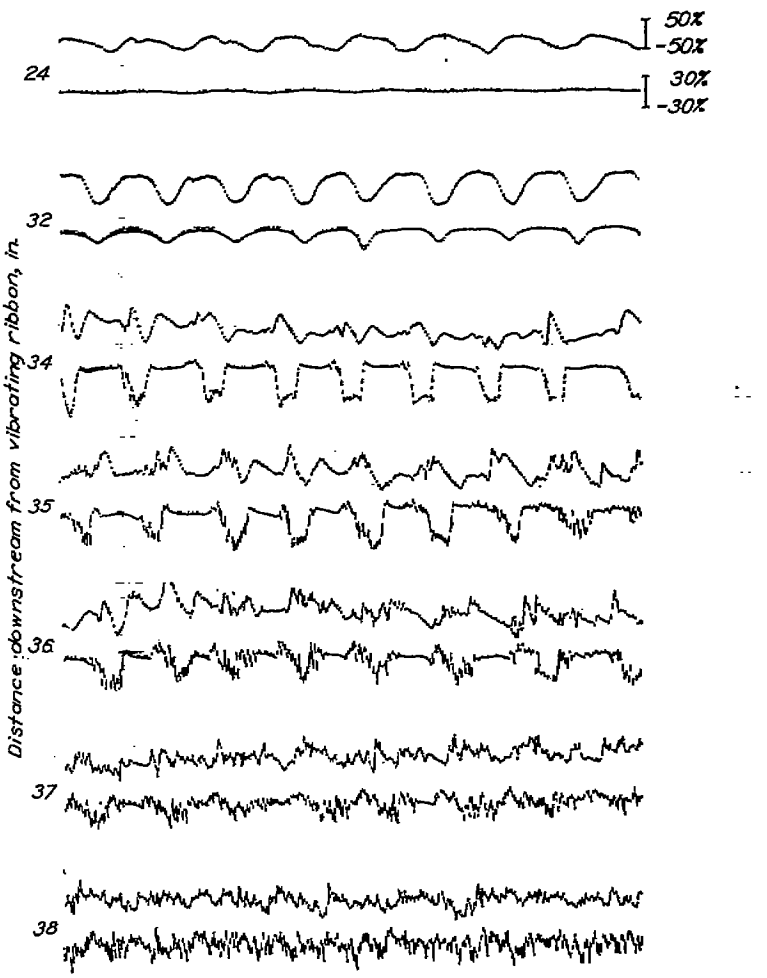

FIGURE 36.—Oscillograms of u-fluctuations showing development of turbulence from oscillations produced by vibrating ribbon. Simultaneous records from two hot wires. Upper trace, hot wire 0.011 inch from surface; lower trace, hot wire 0.112 inch from surface; ribbon 3 feet from leading edge of plate; frequency, 70 cycles per second; U_0=50 feet per second.

remained fixed. Figure 37 shows the same condition but for the two traces photographed separately in order to eliminate the dotting effect of the electronic switch. The difference in the appearance of the records in these two figures is due more to the different magnification than to the character of the traces. Since the frequency of 70 cycles per second is amplified by the boundary layer, the amplitude increases downstream and increasing distance is in one respect like increasing ribbon amplitude in figure 35. The two cases are not equivalent, however, because the boundary-layer thickness increases from record to record in figures 36 and 37.

From calibration data, obtained in connection with figures 36 and 37, it was possible to relate two particular displacements on the record to a percentage change in the mean velocity at the position of the wire. These two percentages are indicated at the right of each trace, an upward displacement indicating an increase and a downward displacement a decrease from the mean local velocity at the hot wire. The percentages are the same for all records in figure 36.

For fluctuations as large as most of those shown, it is not possible to indicate the zero- or mean-velocity position of the trace. This is because of the nonlinear characteristics of the hot wire which produces greater displacements of the

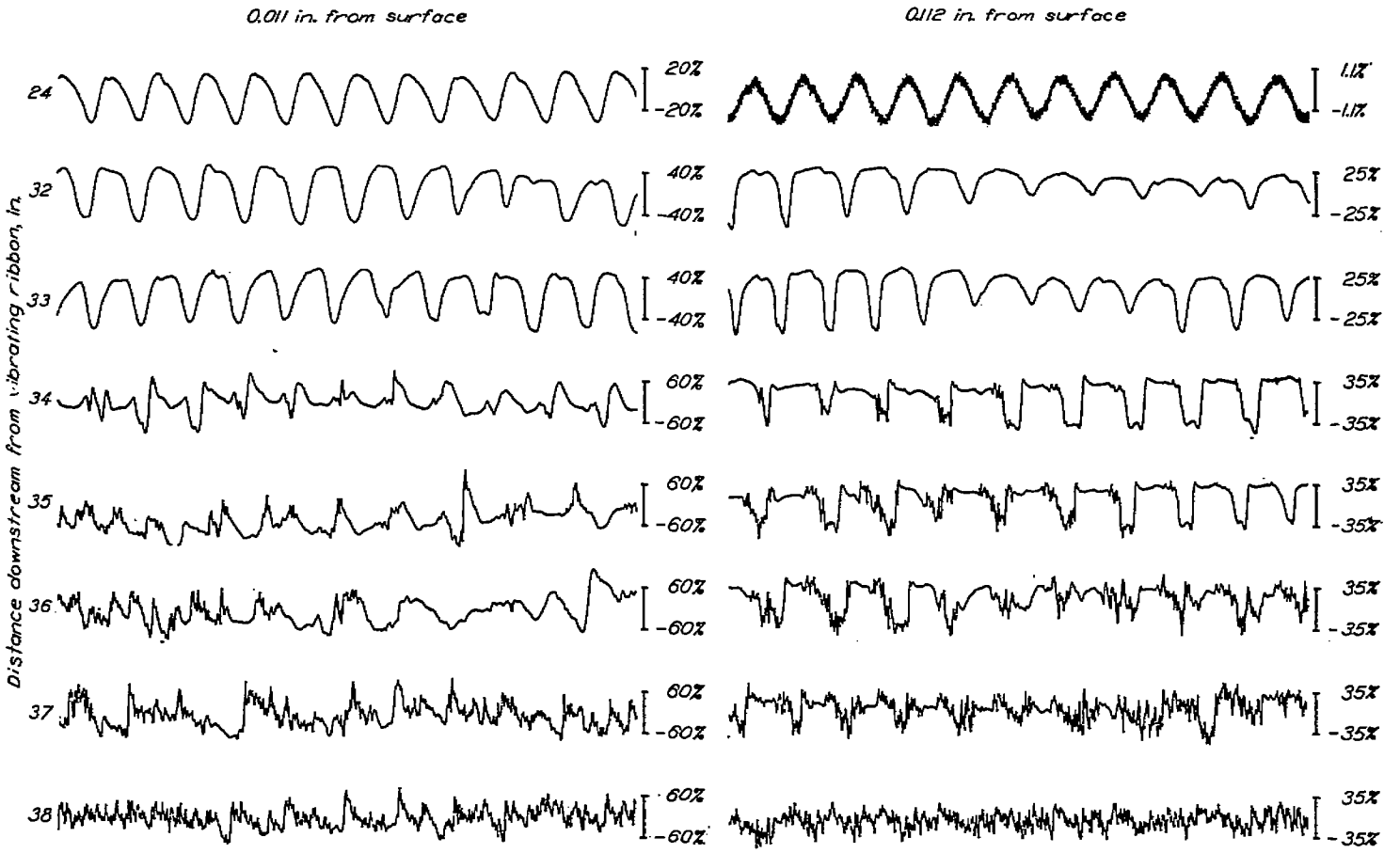

FIGURE 37.—Oscillograms of u-fluctuations showing development of turbulence from oscillations produced by vibrating ribbon placed 3 feet from leading edge of plate. Frequency, 70 cycles per second; U_1=50 feet per second.

trace for velocity decreases than for increases. A certain amount of distortion and some error in the records will result from this effect. It is certain, however, that crests are above the mean velocity while troughs are below the mean and that the distance between the two is approximately the double amplitude. The scale at the right furnishes a measure of the double amplitude.

In the succession of changes occurring from point to point through the transition region, the oscillations first increase in amplitude and, once large, undergo increasing amounts of distortion. Turbulence appears at first in short intervals of the trace and finally for the full length of the trace. Randomness occurs gradually, and this suggests a continuous transition from wave to turbulent motion. It is not difficult to imagine a process here like that often assumed for the formation of eddies from a free vortex sheet. The sheet is imagined to take first a wavelike character, then as the wave grows to curl up into discrete eddies. The disturbed laminar boundary layer may be regarded as a wavy vortex layer with the wave progressively increasing in amplitude and distorting until discrete eddies are formed. The eddies themselves are unstable and soon break up into a diffusive type of motion which characterizes turbulent flow. If the validity of this picture is granted, transition is understood when the wave motion is understood. An understanding of transition is therefore close but only close because the wave motion is understood only when the amplitude is small. Furthermore, the important question concerning where along the surface eddies first form is still unanswered.

Another process may also be imagined. It will be noted in figures 35 to 37 that transition takes place in a more orderly manner at the greater distance from the surface. Here turbulence appears in certain parts of the wave cycle, generally in the sharp-pointed low-velocity part of the cycle. This behavior lends support to the view held by some investigators that transition occurs when the flow comes to rest or reverses direction near the surface (separation point). While the amplitudes shown do not reach the necessary 100 percent, it seems possible that this value would be found at some point nearer the surface. Against this argument is the fact that the records made nearer the surface do not show the turbulent bursts confined to the low-velocity side of the cycle. The argument is further weakened by the possibility of accounting for the observed effects at the greater y-values by the difference between the distribution of mean velocity characteristic of a laminar layer and that characteristic of a turbulent layer. This is to say, that the observed effect is caused by the turbulence rather than a cause of the turbulence.

The idea of transition by separation has been formulated by Taylor (reference 1) by assuming intermittent separation or near separation to be caused by the local pressure gradients accompanying disturbances. The assumption is that separation is imminent when the Kármán-Pohlhausen parameter Λ, derived from pressure gradients either steady or fluctuating, reaches a certain negative value. A steady adverse pressure gradient large enough to cause laminar separation is known to bring about transition rather than complete separation when the Reynolds number is sufficiently high. By analogy,

intermittent separation is supposed to have the same effect. For isotropic turbulence in the surrounding flow the fluctuating pressure gradient is known in terms of measurable quantities, namely, u' and the scale. Taylor's relation is

$$\frac{u'}{U_0}\left(\frac{x}{L}\right)^{1/5}=F(R_x)$$

where L is the scale and $F(R_x)$ expresses a function of the x-Reynolds number of transition.

In essence Taylor's relation rests on the concept of velocity fluctuations impressed on the boundary layer from pressures outside. When velocity fluctuations belong to the natural wave in the boundary layer, Taylor's relation can have little bearing on the problem. There is therefore no theory connecting oscillations to transition. The idea of transition by separation leads to the concept that transition results when the u-component of the wave gets sufficiently large to reverse the flow near the surface. A lack of knowledge regarding large-amplitude waves results in a lack of information concerning the point where transition will occur.

It has not been proved that separation is a necessary condition for transition. Figure 11, where a slight reversal near the surface is indicated by a frequency doubling in the lower part of the cycle in the trace at 4 feet, gives evidence that reversal alone is not a sufficient condition. Perhaps the former picture, based on the analogy to the vortex sheet, is the more accurate one.

Since the Taylor relation is not applicable when transition results from amplified waves, the average scale of the initial disturbance is important only insofar as it is related to the spectrum of the disturbance. The frequency distribution of the initial disturbance is of great importance, since amplification finally selects only a very narrow band of frequencies from all those initially present to bring about transition. The presence or absence of frequencies near this amplified band is obviously more important than the total energy of the disturbance.

Only on the basis of certain prominent frequency bands in the stream turbulence can figure 7 be explained. The reasoning is as follows: If no disturbances were present, theoretically transition should not occur. The pairs of curves in figure 7 should then approach $R_x=\infty$ for zero turbulence. On the basis of amplification of initial disturbances in which all frequencies are present, equation (33) suggests that the curves defining the transition region should fall rapidly at first and then at a progressively diminishing rate as the turbulence is further increased. Actually, the opposite trend is shown in figure 7. Figure 8 shows that not all frequencies are represented alike and, furthermore, that noise is responsible for many of the peaks shown. As the present turbulence was decreased by the addition of damping screens, the ratio of noise to true turbulence was increased. While the total energy of the disturbance was decreased, the energy in certain frequency bands may actually have been increased. A reduction of noise might have greatly altered figure 7.

X. CONCLUSION

Laminar-boundary-layer oscillations are the velocity fluctuations that result from a wave traveling downstream through the boundary layer. The characteristics of this wave have been measured and good agreement with theory has been obtained. The wave may be set up either by a vibrating object in the boundary layer, such as a vibrating ribbon, or by disturbances from the outside, such as stream turbulence and sound. When the disturbance is random or nearly random and contains many frequencies, amplification and damping isolate a wave containing a narrow band of frequencies in the neighborhood of the frequency most highly amplified.

A wave in the boundary layer constitutes a disturbance that will cause transition on a flat plate with zero pressure gradient when the amplitude is sufficiently large. A sufficiently large random disturbance will also cause transition. When random initial disturbances are so small that transition is delayed until values of $R\leqslant 2000$ have been reached, sufficient amplification can occur from the experimentally established lower limit $R=450$, to $R\leqslant 2000$, to give rise to a recognizable oscillation. Larger initial disturbances obscure the oscillations by irregular fluctuations of comparable magnitude.

Natural disturbances may be sound waves as well as turbulence. Turbulence generally has a more nearly random distribution of energy with frequency than sound. In view of the importance of frequency, sound disturbances with a concentration of energy in frequency bands that are highly amplified by the boundary layer may be more conducive to early transition than turbulence. This is important in free flight where turbulence is probably negligible but where engine and propeller noise is present in large amounts.

The effect of pressure gradient on the oscillations is a practicably important phase of the problem about which more should be known. Little more has been done here than to show the direction of the effect and to give some idea of its magnitude. The results are in accord with theory, which also is incomplete in this respect.

Other aspects of the problem remain to be investigated. One of these having practical importance is the effect of curvature. The importance of boundary-layer oscillations on airfoils cannot be determined until effects of curvature as well as pressure gradient are known. Other quantities associated with the wave but not investigated are v and uv. A study of these quantities would be interesting as a further check on the theory, although hardly necessary to identify the oscillations and their characteristics in view of the information derived from studies of u.

It is possible that boundary-layer oscillations may arise from internal disturbances as well as from external disturbances—that is, from surface irregularities and vibration of the surface. A randomly distributed small roughness may produce effects similar to small amounts of turbulence in the air stream. Small ridges or waves in the surface may start oscillations when the spacing is near some amplified

wave length. Vibration of the surface, like sound, may produce oscillations, especially when the frequency is near some amplified oscillation frequency. An investigation of these and other phases of the problem will throw additional light on the important problem of transition.

NATIONAL BUREAU OF STANDARDS,
WASHINGTON, D. C., *April 1943.*

REFERENCES

1. Taylor, G. I.: Statistical Theory of Turbulence. V. Effect of Turbulence on Boundary Layer. Theoretical Discussion of Relationship between Scale of Turbulence and Critical Resistance of Spheres. Proc. Roy. Soc. (London), ser. A, vol. 156, no. 888, Aug. 1936, pp. 307–317.
2. Tollmien, W.: The Production of Turbulence. NACA TM 609, 1931.
3. Tollmien, W.: General Instability Criterion of Laminar Velocity Distributions. NACA TM 792, 1936.
4. Schlichting, H.: Zur Entstehung der Turbulenz bei der Plattenströmung. Nach. Gesell. d. Wiss. z. Göttingen, Math. Phys. Klasse, 1933, pp. 181–208.
5. Schlichting, H.: Amplitudenverteilung und Energiebilanz der kleinen Störungen bei der Plattenströmung. Nach. Gesell. d. Wiss. z. Göttingen, Math. Phys. Klasse, Bd. I, 1935, pp. 47–78.
6. Schlichting, H.: Über die Entstehung der Turbulenz in einem Rotierenden Zylinder. Nach. Gesell. d. Wiss. z. Göttingen, Math. Phys. Klasse, Heft 2, 1932, pp. 160–198.
7. Schlichting, H.: Turbulenz bei Wärmeschichtung. Z. f. a. M. M., Bd. 15, Heft 6, Dec. 1935, pp. 313–338.
8. Rosenbrook, G.: Instabilität der Gleitschicht im schwach divergenten Kanal. Z. f. a. M. M., Bd. 17, 1937, pp. 8–24.
9. Hollingdale, S. H.: Stability and Configuration of the Wakes Produced by Solid Bodies Moving through Fluids. Phil. Mag., ser. 7, vol. 29, no. 194, March 1940, pp. 211–257.
10. Savic, P.: On Acoustically Effective Vortex Motion in Gaseous Jets. Phil. Mag., ser. 7, vol. 32, Sept. 1941, pp. 245–252.
11. Dryden, Hugh L.: Air Flow in the Boundary Layer near a Plate. NACA Rep. 562, 1936.
12. Nikuradse, J.: Experimentelle Untersuchungen zur Turbulenzentstehung. Z. f. a. M. M., Bd. 13, Heft 3, June 1933, pp. 174–176.
13. Fluid Motion Panel of the Aeronautical Research Committee and Others: Modern Developments in Fluid Dynamics. Vol. I, S. Goldstein, ed., The Clarendon Press (Oxford), 1938, p. 136.
14. Mock, W. C., Jr.: Alternating-Current Equipment for the Measurement of Fluctuations of Air Speed in Turbulent Flow. NACA Rep. 598, 1937.
15. Mock, W. C., Jr., and Dryden, H. L.: Improved Apparatus for the Measurement of Fluctuations of Air Speed in Turbulent Flow. NACA Rep. 448, 1933.
16. Dryden, H. L., and Kuethe, A. M.: The Measurement of Fluctuations of Air Speed by the Hot-Wire Anemometer. NACA Rep. 320, 1929.
17. Dryden, Hugh L., Schubauer, G. B., Mock, W. C., Jr., and Skramstad, H. K.: Measurements of Intensity and Scale of Wind-Tunnel Turbulence and Their Relation to the Critical Reynolds Number of Spheres. NACA Rep. 581, 1937.
18. Hall, A. A., and Hislop, G. S.: Experiments on the Transition of the Laminar Boundary Layer on a Flat Plate. R. & M. No. 1843, British A. R. C., 1938.
19. Dryden, Hugh L.: Turbulence Investigations at the National Bureau of Standards. Proc. Fifth Int. Cong. Appl. Mech., (Sept. 12th-16th, 1938, Cambridge, Mass.), John Wiley & Sons, Inc., 1939, pp. 362–368.
20. Prandtl, L.: The Mechanics of Viscous Fluids. Vol. III of Aerodynamic Theory, div. G, W. F. Durand, ed., Julius Springer (Berlin), 1935.
21. Rayleigh, Lord: On the Stability or Instability of Certain Fluid Motions. Proc. London Math. Soc., vol. 11, 1880, pp. 57–70; and vol. 19, 1887, pp. 67–74.
22. Tietjens, O.: Beiträge zur Entstehung der Turbulenz. Z. f. a. M. M., Bd. 5, Heft 3, June 1925, pp. 200–217.
23. Görtler, H.: Über den Einfluss der Wandkrümmung auf die Entstehung der Turbulenz. Z. f. a. M. M., Bd. 20, Heft 3, June 1940, pp. 138–147.
24. Pretsch, J.: The Stability of Laminar Flow past a Sphere NACA TM 1017, 1942.